On the theory of SODAR measurement techniques

Antoniou, I.; Ejsing Jørgensen, Hans; Bradley, S.

Publication date:
2003

Document Version
Publisher's PDF, also known as Version of record

Risø-R-1410(EN)

On the Theory of SODAR Measurement Techniques

(final reporting on WP1, EU WISE project NNE5-2001-297)

Ioannis Antoniou (ed.), Hans E. Jørgensen (ed.)
(Risoe National Laboratory)
Frank Ormel
(ECN, Energy research Center of the Netherlands)
Stuart Bradley, Sabine von Hünerbein
(University of Salford)
Stefan Emeis
(Forschungszentrum Karlsruhe GmbH)
Günter Warmbier
(GWU-Umwelttechnik GmbH)

Risø National Laboratory, Roskilde, Denmark
April 2003

Abstract

The need for alternative means to measure the wind speed for wind energy purposes has increased with the increase of the size of wind turbines. The cost and the technical difficulties for performing wind speed measurements has also increased with the size of the wind turbines, since it is demanded that the wind speed has to be measured at the rotor center of the turbine and the size of both the rotor and the hub height have grown following the increase in the size of the wind turbines. The SODAR (SOund Detection And Ranging) is an alternative to the use of cup anemometers and offers the possibility of measuring both the wind speed distribution with height and the wind direction.

At the same time the SODAR presents a number of serious drawbacks such as the low number of measurements per time period, the dependence of the ability to measure on the atmospheric conditions and the difficulty of measuring at higher wind speeds due to either background noise or the neutral condition of the atmosphere.

Within the WISE project (EU project number NNE5-2001-297), a number of work packages have been defined in order to deal with the SODAR. The present report is the result of the work package 1. Within this package the objective has been to present and achieve the following:

- An accurate theoretic model that describes all the relevant aspects of the interaction of the sound beam with the atmosphere in the level of detail needed for wind energy applications.
- Understanding of dependence of SODAR performance on hard- and software configuration.
- Quantification of principal difference between SODAR wind measurement and wind speed measurements with cup anemometers with regard to power performance measurements.

The work associated to the above is described in the work program as follows:

a) Draw up an accurate model of the theoretic background of the SODAR. The necessary depth is reached when the influences of various variables in the model on the accuracy of the measurement have been assessed.
b) Describe the general algorithm SODAR uses for sending the beam and measuring the reflections. Describe the influence of various settings on the working of the algorithm.
c) Using the data set from work package two analyse the differences between point measurements and profile measurements.

All the above issues are addressed in the following report

ISBN 87-550-3217-6
ISBN 87-550-3218-4 (Internet)
ISSN 0106-2840

Print: Pitney Bowes Management Services Denmark A/S, 2003

Contents

1. Preface

The usage of wind energy is essentially the usage of the kinetic energy contained in an atmospheric volume that passes through the rotor plane during a certain time interval. Thus the perfect wind measurement for wind energy purposes would be a plane-integrated wind detection with high temporal resolution. As such measurements are not possible they are usually substituted by point measurements at hub height (often even at lower heights and then extrapolated to hub height) or by volume measurements with remote sensing devices from the ground.

The volume measurements by remote sensing devices (SODAR. LIDAR, RASS, etc.) have a great advantage compared to point measurements in one height: they yield information from different heights simultaneously (tethered balloons would give such data only sequentially). Thus we get a wind profile vertically across the rotor plane. The necessity to vertically interpolate (or even worse extrapolate) wind speed and variance is no longer required.

In the following we deal with the issues of SODAR algorithms, the differences between point and volume measurements and some comparisons are made. After this discussion we investigate the advantages of a profile measurement compared to extrapolations from a point measurement and the SODAR results are compared to the results of a cup anemometer as far as the issue of the measurement principle is concerned. Finally the influence of the wind shear and the atmospheric turbulence is discussed in connection to their influence on the wind turbine performance and a relevant example is given in order to quantify this influence.

2. SODAR algorithms

This chapter deals with the "standard" SODAR algorithms. It is not aimed at a specific make of SODAR but generalised to be valid for general phased array SODARs. The chapter is divided in four parts: general, beam sending, signal receiving and parameter interdependence.

The general part introduces some general ideas of the interactions between the SODAR and the atmosphere. The sending and receiving are focussed on sending the beam and receiving the backscattered signal and the last part (parameter interdependence) explains the relations between a number of variables encountered earlier.

The aim of this chapter is

- to give insight into the conditions that affect the SODAR,
- to show how the settings can change the measurement results and
- to give a basic understanding of the relationships between settings in order for the reader to be able to make a complete set of SODAR settings that takes these interdependencies into account.

2.1 Generally on phased array SODARS

To measure the wind profile with a SODAR, acoustic pulses are sent vertically and at a small angle to the vertical. A thus transmitted sound pulse is scattered by fluctuations of the refractive index of air. Those fluctuations can develop through temperature and humidity fluctuations and gradients as well as wind shear. Due to the scattering angle of 180°, the commercially available monostatic SODARS are mainly sensitive to the thermal fluctuations. As reflected sound intensity depends strongly on the size of the fluctuations, scattering is restricted to turbulent patches of size $\lambda/2$. In other words changes of the transmitted sound frequency lead to scattering from differently sized fluctuations.

Turbulent fluctuations move with the wind. Therefore the Doppler effect shifts the sound frequency during the scattering process. The amount of frequency shift is proportional to the velocity of the scatterer in the beam direction. If the beam is directed vertically, the vertical wind speed w can be calculated directly from the Doppler shift. The horizontal components however need to be determined by tilting the beam also by a small angle θ_0 from the vertical into two horizontally perpendicular

directions whose wind components we will call *u* (East) and *v* (North). This gives three Doppler shifts, which are a function of the wind components *u*, *v*, and *w*.

The pulse is assumed to be confined to a conical beam of half-angle θ. For a system having pulse duration τ and with speed of sound *c* , the pulse is spread over a height range of $c\tau$. As the pulse is scattered, it is detected at any one time from a volume $V = \pi\left(z\theta\right)^2 c\tau/2$ where $c\tau/2$ is the height range and $\pi(z\theta)^2$ is the horizontal extension with z being the height above the antenna array.

Note that the centres of the scattering volumes for the three beams are separated by a horizontal distance of up to 88m at a typical tilt angle of θ_0 = 18° and a range of 200 m. At the same time the horizontal beam cross section is 35 m. This means that two respective scattering volumes do not even overlap. Therefore the assumption of homogeneous turbulence and a homogeneous wind field within the volume of all three beams is necessary.

Even if turbulence is strong the scattered signal power is extremely weak in comparison to the transmitted power: The ratio between received and transmitted powers at a height of a 100 m above ground and for a 4500 Hz SODAR is typically of the order of 10^{-14} Therefore absorption in the atmosphere is an important factor restricting the range that is the maximum height from which scattered signals can be detected. The SODAR equation (Eq. 1) shows that the ratio of received to transmitted power is proportional to the absorption term: $\frac{P_R}{P_T} \propto e^{-2\alpha z}$

The absorption coefficient α is the sum of classical absorption, α_c, and molecular absorption, α_m. Classical absorption is due to viscous losses when sound causes motion of molecules, and is proportional to frequency squared. Molecular absorption is due to water vapour molecules colliding with oxygen and nitrogen molecules and exciting vibrations, which are dissipated as heat. At low humidity there is little molecular absorption. At high humidity O_2 and N_2 molecules are fully excited without acoustically enhanced collisions, and there is again little extra absorption. Absorption also depends on temperature and pressure since these affect collisions. The resulting equation shows a complicated dependence on the mentioned parameters as well as on the sound frequency. However, in the frequency range of interest for SODARS that is between 1 and 10 kHz the following rule is valid: The higher the frequency of a SODAR the more limited its range due to absorption. For a detailed treatment of sound absorption in air see Salomons, E. M. (2001)

2.2 Beam Sending:

There are five basic parameters that determine how the SODAR sends the beam. These are:

1. Transmit frequency (f_T)
2. Transmit power (P_T)
3. Pulse length (τ)
4. Rise time (up and down) (βτ)
5. Time between pulses (T)

There are some further parameters necessary to describe the three different beams of the antenna but these depend on other parameters and cannot be set. These further parameters are:

6. The tilt angle
7. Half beam width

The following drawing shows the relationship between these parameters. The basic pulse shape is shown in Figure 1 and the pulse repetition pattern in Figure 2.

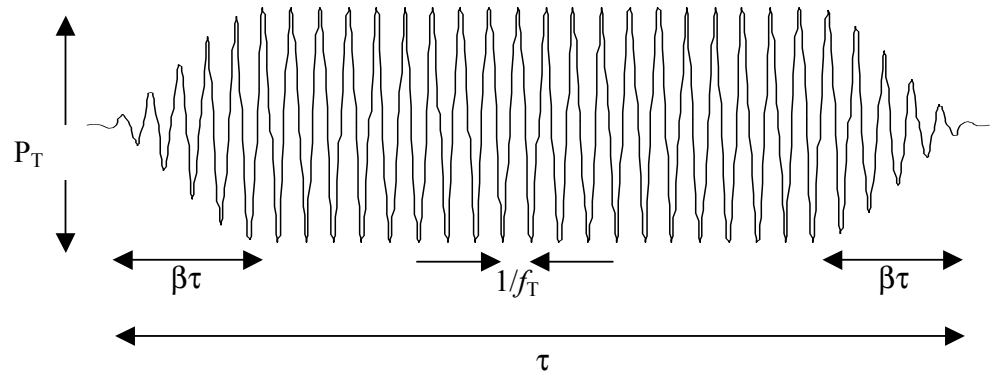

Figure 1 Basic pulse shape of the SODAR

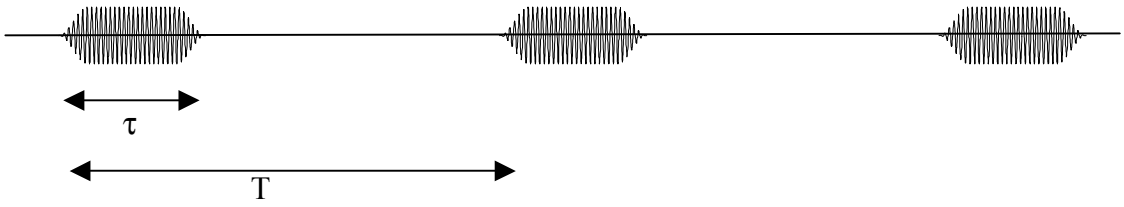

Figure 2 The pulse repetition

2.2.1 Frequency

The frequency of a standard phased array sodar is determined in the design process. There is little room for changing the frequency once the SODAR has been assembled. For example, a 4500 Hz mini SODAR can usually be adjusted between 3000 and 6000 Hz. Outside this frequency band the loudspeaker performance is too bad to be used. For lower frequencies the bandwidth is generally smaller such as 1500-2500 Hz (for a SODAR that is normally operated at 2000 Hz). The choice for the frequency is a basic parameter in the maximum altitude reached. This is because the background noise decreases when the frequency increases but the absorption in the atmosphere increases with frequency: The atmospheric absorption basically depends on three parameters: temperature T, relative humidity RH and frequency f. Of these three only the frequency is a design parameter for the SODAR. In Figure 3and Figure 4can be seen that the absorption increases exponentially with the frequency. This limits the maximum height that the SODAR can reach.

On the other hand the background noise level tends to decrease with increasing frequency, especially during the day. This can be seen in Figure 5. A lower background noise level for a specific frequency would mean that the SODAR can reach a higher altitude with the measurements.

From these two considerations can be concluded that there is an optimal frequency depending on the application. A last point to be considered in the choice of frequency is the radial wind speed resolution, which depends on the frequency. The formulas can be found later in this chapter, but the higher the frequency, the better the resolution. This can be influencing the choice for a higher frequency, which means lower sampling depth but higher resolution.

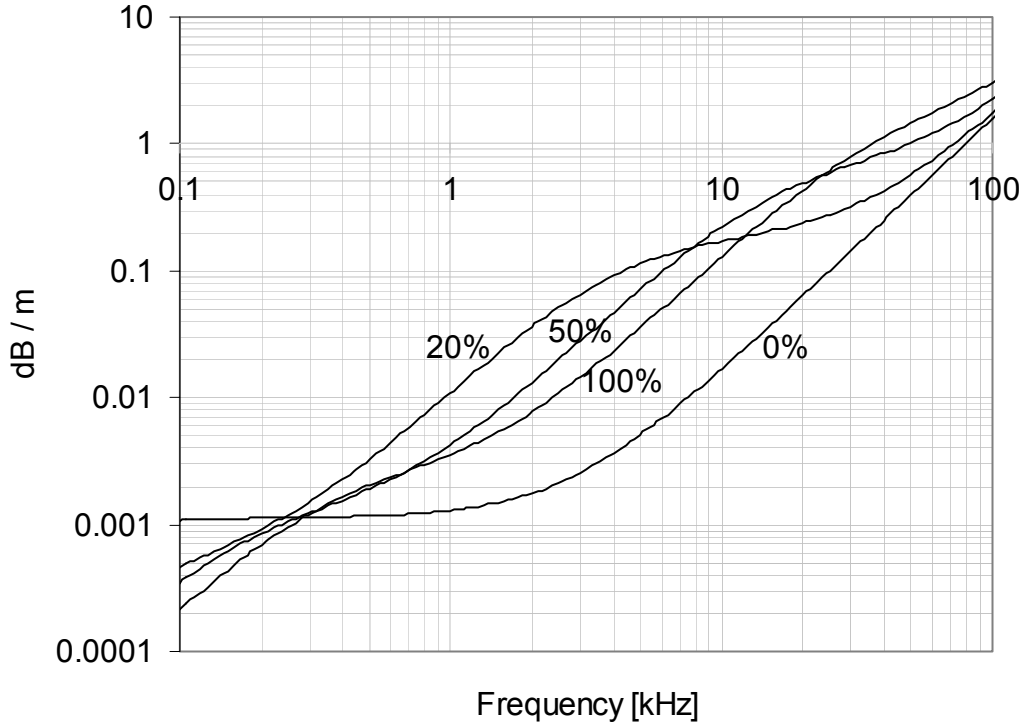

Figure 3 Atmospheric absorption (at T = 283 K) for different values of Relative Humidity.

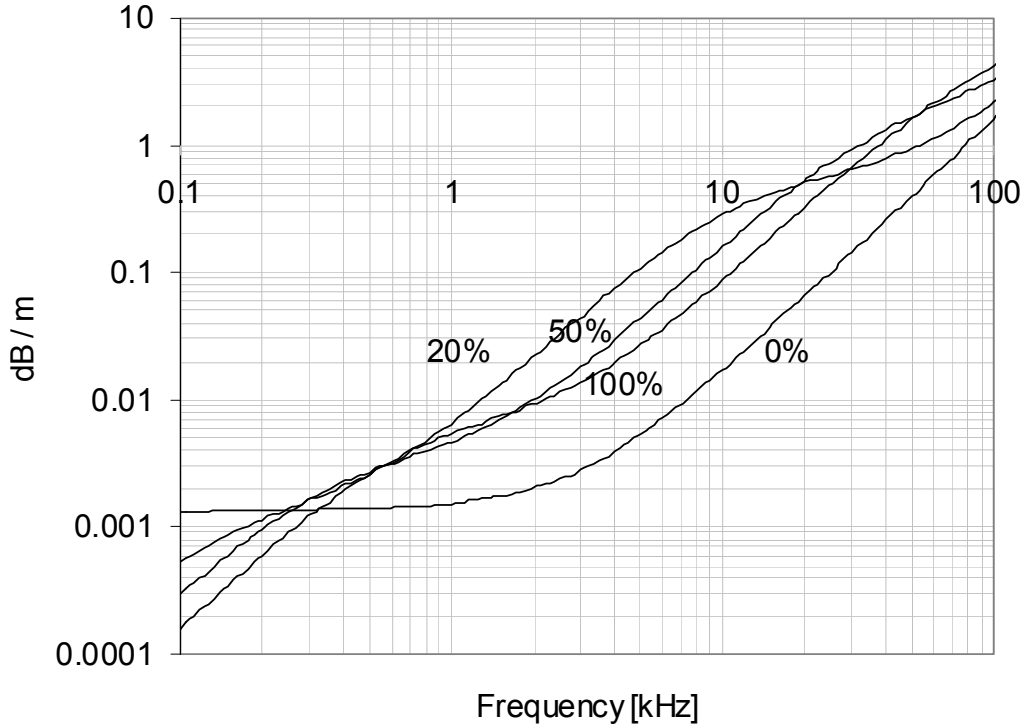

Figure 4 Atmospheric absorption (at T = 293 K) for different values of Relative Humidity.

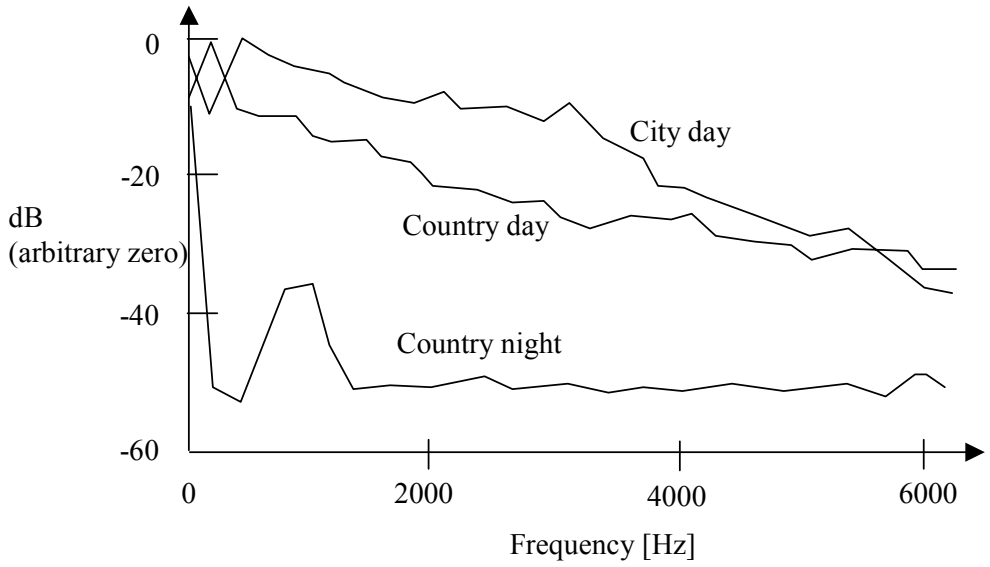

Figure 5 Background noise levels for different surroundings

2.2.2 Power

This is one of the simpler parameters: the power should be set to such a level that the speakers just are not damaged by the voltage signal. This can be clearly seen from the SODAR equation:

$$P_R = P_T G A_e \sigma_s \frac{c\tau}{2} \frac{e^{-2\alpha z}}{z^2} \qquad \text{(Eq. 1)}$$

With
- P_T the transmitted power
- G the antenna transmitting efficiency
- A_e the antenna effective receive area
- τ the pulse duration
- z the height
- α the absorption of air
- σ_s the turbulent scattering cross section
- c the wind speed in air ($\pm$ 340 m/s)

The more power is put into the beam, the more power is received back. Therefore the only consideration is how much power the speakers can deliver without damage.

2.2.3 Pulse length

The pulse length is the length of the pulse (either in milliseconds or in meters). Normally only the effective pulse width with respect to power output is used in calculations; this is the pulse width without the rise time plus half the rise time (up and down). So a pulse length of 100 ms with a rise time (up and down) of 15%, will have an effective pulse length of 85 ms.

The pulse length influences the following:

- power received from the atmosphere from Sodar equation (Eq. 1, longer transmit pulse means more received power)
- $$\frac{P_R}{P_T} \propto \tau \qquad \text{(Eq. 2)}$$
- frequency resolution (and therefore radial wind speed resolution)

- $\Delta f_V = \frac{1}{\tau}$ (Eq. 3)

- height resolution

- $\Delta z = \frac{c\tau}{2}$ (Eq. 4)

2.2.4 Rise time

The rise time means that the signal is attenuated by a Hanning filter, which means it gets a ramp up and ramp down at the beginning and end of the signal. This protects the speakers from too quick rise in voltage which could damage them. Assuming a pulse shape $p(t)$ and duration τ, determining the Hanning shape is defined as follows:

$$(1-\beta)\,p(t) = \begin{cases} \frac{1}{2}\left[1-\cos\left(\frac{\pi}{\beta\tau}t\right)\right] & 0 < t < \beta\tau \\ 1 & \beta\tau < t < \tau(1-\beta) \\ \frac{1}{2}\left[1-\cos\left(\frac{\pi}{\beta\tau}\{\tau - t\}\right)\right] & \tau(1-\beta) < t < \tau \end{cases} . \quad \text{(Eq. 5)}$$

Time series of the pulse shapes are shown in Figure 6, for β = 0, 0.2, and 0.5. The pulses become more round with increasing β. The frequency spectra for these three pulse shapes are shown in Figure 7 (in practice the pulse is the *product* of the envelope and a sine wave at the transmit frequency f_T, and so the pulse spectrum is *convolved* with a spectrum line at f_T, and so has the shape shown centred on f_T).

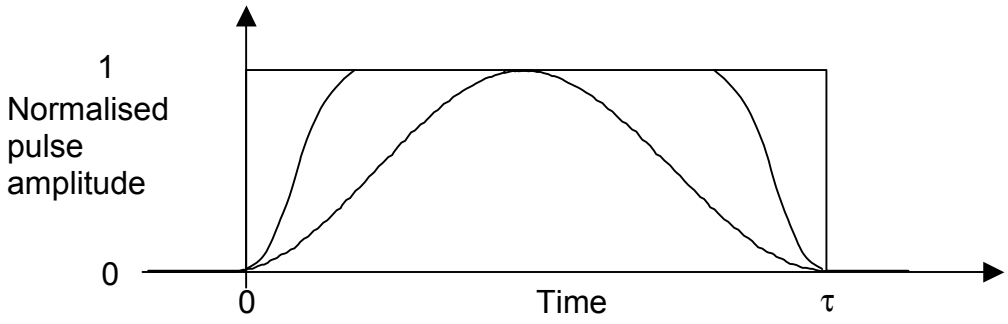

Figure 6 Time series of square window compared to Hanning shaped pulse with different ramp times.

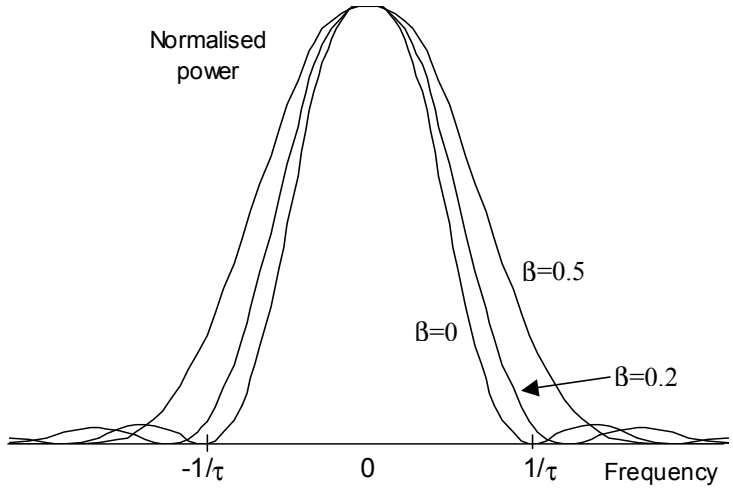

Figure 7 Frequency spectra of a square pulse compared to Hanning shaped pulse with different ramp times.

An ideal pulse (β=0) would have all the energy in the main lobe of the sine function (around the y-axis) and decay to zero with no ripples. However, the rectangular pulse introduces ripples into the frequency domain. These are unwanted contributions, which could be aliased back into the spectrum.

With increasing β, the pulse has a broader and deeper main lobe, which means that more of the energy is in this main lobe and less is in the ripples. If there is less energy in the ripples then it means that the frequency response will also have less ripples, therefore a better function for windowing data. The broadening of the main lobe is unwanted as the transmit frequency is less well defined.

Therefore, the user needs to find a trade-off between "ripples", pulse power, and well defined transmit frequency.

2.2.5 Time between pulses

There is a direct relation between the time between pulses T and the maximum height the SODAR attempts to measure. Any measurement of backscatter must be finished before the next pulse is sent, therefore the maximum height is cT/2.

Another consideration is the danger of getting backscatter from the previous pulse in the measurements. If the SODAR has a general sampling depth of 500 metres, and the maximum height is set at 150 metres, then we get the following situation:

If we assume that the phased array sodar has three beams, then it will listen to backscatter from one beam for 0.88s. After this 0.88s it will do the same for the other two beams. So after 2.65s it will come back to the first beam. When it starts to listen for the backscatter from the second pulse of the first beam (2.65s after the first pulse was sent) then there will also be backscatter from 450 metres high. This means that the wind speed at 450 to 600 metres is represented as wind speed for 0 to 150 metres. But also the backscatter from the second pulse will give a wind speed for these altitudes, and so there will be two peaks in the spectrum. This is a very unwanted situation that can spoil the measurements. As a rule of thumb the maximum height should be set to ½ or ⅔ the maximum sampling depth the SODAR can reach. As this maximum depth depends on the atmospheric boundary layer, it is best to set the maximum height to a value on the safe side.

2.2.6 The tilt angle

Although the tilt angle of the U and V beam relative to the W beam is important to know in order to be able to calculate the wind speed, it is not a parameter that can be set by software. The tilt angle θ is defined by the loud speaker spacing d of the antenna array, by the number of speakers N and by the

transmit frequency f (or wavenumber k). The resulting intensity pattern can be compared to optical interference patterns:

$$I \propto \left[\frac{\sin\left(Nk\frac{d}{2}\sin\theta \right)}{\sin\left(k\frac{d}{2}\sin\theta \right)} \right]^2 \qquad \text{(Eq. 6)}$$

This is the intensity for a loudspeaker array of N speakers in a line showing the general principle. An example for 8 speakers and two different tilt angles (vertical – thick line, 15˚ from vertical – thin line) is shown in Figure 8.

Note that there is a second maximum as high as the first at about 95˚ from the main lobe. There are two important issues connected with this second maximum:

a) the second maximum could lead to strong reflections from surrounding hard objects like buildings, tarmac, and trees. This is prevented by a SODAR baffle which is a sound absorbing shield inside the SODAR enclosure.
b) b) the second maximum restricts the tilt angle: If the main beam is tilted too much then the second maximum acts as a new main beam and the scattered signal becomes ambiguous.

Theoretically, the beam could be steered by a variable phase-shift between 0 and π/2 between two respective loudspeaker groups. To simplify the design however, SODAR manufacturers fix the progressive phase-shift at π/2. In practice this leads to tilt angles of 16° - 30° for higher to lower transmit frequencies respectively. The practical limit on the beam tilt angle is

$$\Delta\theta_{tilt} \leq \frac{2\pi}{4dk} \qquad \text{(Eq. 7)}$$

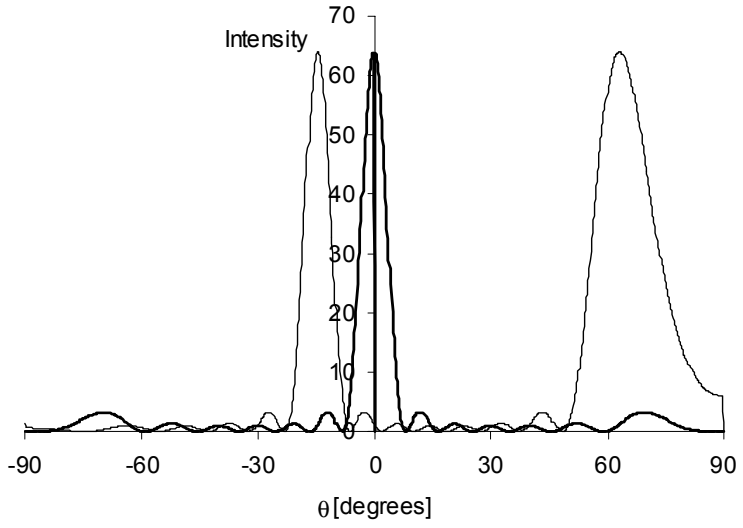

Figure 8 Antenna beam pattern for a line array consisting of 8 speakers with a speaker spacing of 0.95λ and at a transmit frequency of 4500 Hz. The vertical beam corresponds to the thick line, the tilted beam to the thin line.

2.2.7 Half beam width

A final aspect of the beam being sent up that should be discussed is the half beam width. This is also not a parameter that can be set, but it follows from the speaker, array and baffle design.

Again the transmit frequency determines the beam opening angle as can be seen in Figure 9. This is the same linear array consisting of 8 speakers as in Figure 8. The transmit frequencies are 4500 Hz (blue) and 2000 Hz (green) for constant speaker spacing which is unrealistic as speakers for a 2000 Hz SODAR are larger and thus have to be spaced wider. However, it can be seen that the beam-opening angle roughly doubles.

In effect spectral broadening results from and is proportional to the finite beam width. The broadening may be of the same order as finite pulse effects. However, the finite-beam broadening is different, in that it scales with the wind speed.

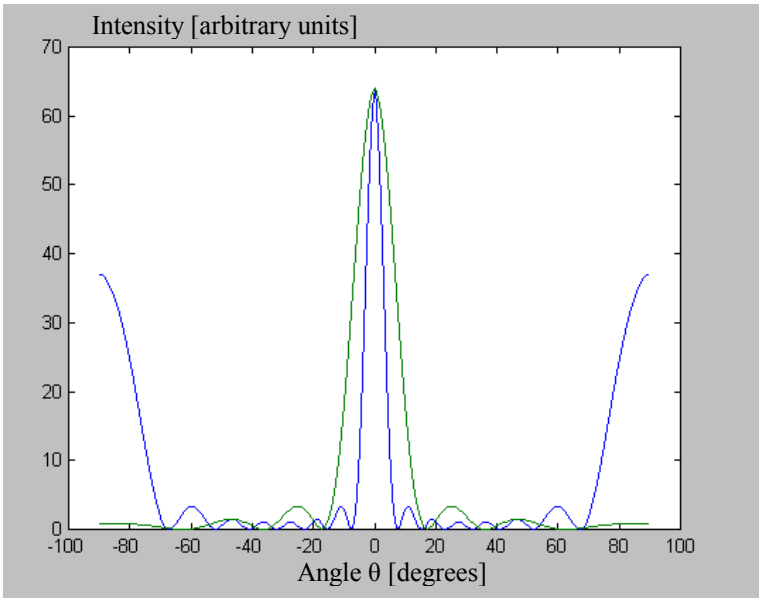

Figure 9 Antenna beam pattern (for details see Fig. 6) at two different transmit frequencies: Blue – 4500 Hz, green – 2000 Hz.

Finally it should be mentioned that the SODAR baffle, which was mentioned in 2.2.6, adds an extra level of complexity to the intensity pattern as it acts as an additional circular hole with its own diffraction pattern. A more realistic example with the transmit frequency f_T = 2 kHz, and the array diameter $2a$ =1 m is given in Figure 10. In this case, the angle plotted is $\theta^* = \theta - \tan^{-1}(a/h)$ with the baffle height h. The intensity at low elevation angles is around 25 dB below that of the main vertical beam.

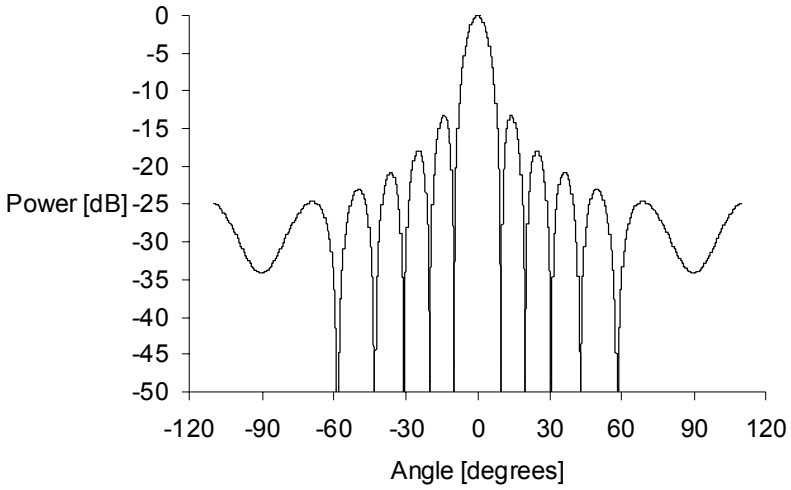

Figure 10 Antenna beam pattern with baffle.

For phased array SODARs, the baffle needs to have a wider exit so that tilted beams do not intersect the baffle edges too much. The top rim of the baffle will be in the near field of the SODAR beam (rays from different parts of the antenna to a point on the rim will not be parallel). However, detailed calculations have shown that the far-field approximations applied above are generally sufficient to optimise a design. Baffles can have a circular cross-section or be some polygon: for the following we just consider the rim as if it were a circle.

The height of the baffle has to be chosen with care, as the enhanced diffraction at the rim of the baffle can lead to enhanced sensitivity to the reflection from surrounding hard objects. The optimum baffle height is determined by:

$$\frac{a}{h} = \tan\theta_{\min} \qquad \text{(Eq. 8)}$$

Where θ_{min} is the angle where the antenna pattern has its first minimum. Unfortunately, this angle changes with both, transmit frequency and tilt angle. Therefore baffle design is still mostly empirically done in practice.

2.3 Signal receiving

After the beam has been transmitted it interacts with the atmosphere. This is described in another chapter in this report. This second section deals with what happens when the backscattered signal reaches again the speakers. These speakers have now been switched and act as microphones. In the following section, the parameters related to the receiving of the backscattered signal will be explained.

2.3.1 The hardware sequence:

The following hardware components can be identified in the receive chain:

1. Microphone
2. Low noise amplifiers
3. Bandwidth filters
4. Ramp gain
5. Mixer
6. Low pass filter

2.3.1.1 Low noise amplifier:

When the backscattered signals reach the speakers (now acting as a microphone), the typical signal strength that the microphones produce is 0.1 to 1 mVrms. This means that an amplification of around 1.000.000 times is needed to get a signal strength of around 1Vrms.

2.3.1.2 Bandwidth filter

After the amplification, the noise has to be filtered out. This is done because only a small part of the frequency spectrum contains meaningful backscatter information but most of the spectrum contains noise. If we filter out this noise then we can get a cleaner spectrum later. The bandwidth that is necessary depends on the maximum wind speed to be measured. The typical value of around 400 Hz on each side of the transmitted frequency corresponds to a wind velocity of about ± 15 m s^{-1} along the beam. As even the tilted beams have a huge vertical component and tend to be in the order of 1 m s^{-1} of horizontal winds, actual measurable horizontal winds can be of the order of 50 m s^{-1}. This example was chosen for a transmit frequency of 4500 Hz and a tilt angle of 16°.

2.3.1.3 Ramp gain

The received signal decreases with the distance it travelled in the atmosphere. Therefore the backscatter that returns from higher altitudes is both weaker and later in time. A ramp gain is therefore introduced which amplifies the signals from higher altitudes more than it amplifies signals from lower altitudes.

2.3.1.4 Mixer

To keep the sampling rate down, the frequency of the signal is mixed down from around the sending frequency to around zero. If before mixing the interesting frequency range is from 4300 Hz to 4700 Hz (with a sending frequency of 4500 Hz) then after the down mixing this interesting frequency range will be from 0 to 200 Hz. In this case the difference between a positive and a negative Doppler shift is indicated by the in-phase trace and the 90° phase trace. As such, it is possible to distinguish between positive and negative Doppler shift also after down mixing.

2.3.1.5 LP filter

After the mixing a low pass filter is applied in order to remove all the higher frequency components still present in the signal. After the LP filter the frequency content in the signal represents the Doppler shift in the received signal. The LP filter therefore also limits the maximum wind speeds that can be seen with the SODAR.

2.3.2 Switching time

When the transducers are switched from speaker to microphone, the main problem is that the transmitted noise will "ring" for some time in the antenna and enclosure. During this time signal levels from ringing are higher than from backscattered signals from the atmosphere and this makes it very difficult to measure meaningful data from low altitudes. Even though the antenna and enclosure is designed to reduce this ringing time by using "soft" materials and acoustic foam in the enclosure, the ringing can affect data quality for the lowest 6 – 10 m (at a pulse length of 40 ms). A typical transient from an Aerovironment SODAR can be seen in the next figure:

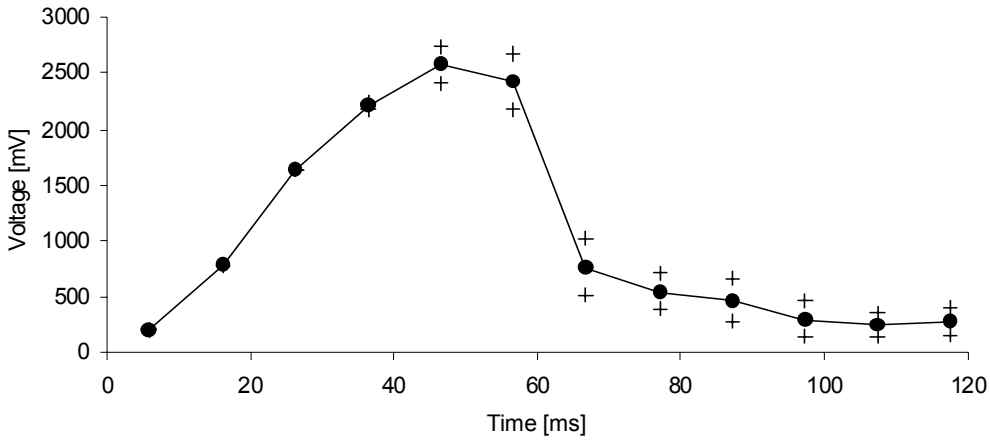

Figure 11 Transducer signal due to ringing where time = 0 ms is the time when the pulse has finished being sent.

2.3.3 Sampling time

The maximum height is defined by the time the SODAR measures backscattered signals. To measure up to a height of 200 meters, the SODAR will have to measure during 1.2 seconds. This sampling time should not be set too short, as otherwise the possibility exists that backscattered signals from a certain pulse will contaminate the signal from the next pulse.

2.3.4 Range gates

The SODAR measures wind speeds at various heights. These heights are also called range gates. The maximum resolution that can be obtained for these range gates is given by two formulas:

$$\Delta z_V = \frac{c\tau}{2} \qquad \text{(Eq. 4)}$$

$$\Delta z_V = \frac{cN_s}{2f_s} \qquad \text{(Eq. 9)}$$

With Δz_V the height resolution, c the sound speed in the air, τ the pulse length in m, Ns the number of samples of an FFT in a time series, and *fs* the sampling rate.

Equation 4 represents the maximum height resolution due to the pulse length whereas Equation 9 represents the maximum height resolution due to the FFT sampling.

The maximum height resolution is equal to the larger value of Δz_V in the above formulas. Often SODARs will present data at finer spatial resolution. This can be done either by doing FFTs using overlapping sequences of samples or by using a higher sampling rate if resolution is limited by Eq. 9. While this may look good on a profile plot, no extra information is gained.

2.3.5 FFT

When the backscattered signal has been sampled, an FFT is done. This FFT is usually done with either 64 or 128 points, at a sampling rate of normally 960Hz. The spectral resolution is 15 Hz (64 points over 960 Hz) which corresponds to a wind speed resolution of 0.55 m s^{-1} along the beam. The sampling frequency also determines the range of wind speeds that can be measured along the beam (f_s = 960 Hz: v_{max} = ± 18 m s^{-1}). As we have seen earlier this amounts to horizontal winds of more than 50 m s^{-1} for a transmit frequency of 4500 Hz and a tilt angle of 16°.

2.3.6 Peak detection

Once the FFT is done for a specific height, the frequency of the peak has to be determined. The following methods can be used to determine peaks:

- By determining the average noise level of that part of the spectrum where no wind speed signal is expected, the background noise can be estimated. The peak is determined through its height above the background noise level
- Averaging of power spectra can also be used. Averaging will not change the signal. The noise (because it is random) will be reduced by the square root of the number of averaged spectra.
- Very often the wind speed is not exactly zero, and reflections from hard objects (fixed echoes) will always be at zero frequency shift. Therefore very often peaks at zero Doppler shift can be ignored.
- The spectrum can be fitted with a specific shape. Based on knowledge of pulse length and other characteristics, this shape can be determined. The part of the spectrum that gives the best fit is the most likely position of the peak.

2.3.7 Consistency checks

If the wind speed is calculated from the instantaneous peaks detected from the spectra, one important problem becomes apparent: The higher the range gate the lower is the signal-to-noise ratio as the sound is absorbed in air and the scattered power decreases. This result in erroneous peak positions from the peak finding algorithm and the resulting wind profiles look “jumpy” both in space and in time. Therefore, it is very common to apply consistency checks and/or averaging. As the essence of a good SODAR system is in how it handles data quality and consistency in a noisy environment, not much is know about the algorithms and techniques actually employed by the manufacturers. However, there are some typical techniques that are commonly used in research instruments and it is therefore likely, to find those in commercial systems as well:

The easiest technique is a straight geometrical average over either the calculated wind profiles or over the Doppler shift along the beam. How to do that will be explained in the section about wind component calculation, as it is very important for the actual information content of the resulting data

set. The user can usually choose the averaging time. Typical values range between 1 minute and 60 minutes.

Alternatively, a moving average can be applied where the profiles become interdependent. Although the resulting wind field looks smoother to the eye, no new information is obtained.

Real consistency checks assume that there is certain inertia of wind profiles in time or a maximum vertical wind shear that is physically possible. In this case for each range gate of a profile the wind or frequency shift can be compared with one or more previous profiles and if a certain maximum difference is exceeded the respective value can either be rejected or smoothed out. The same principle applies to the vertical consistency check where a value is compared with one or more upper and lower neighbours and a certain maximum wind shear is defined. If some level of sophistication is applied the difference values are scaled with the wind speed.

In practice it is likely, to find every possible combination of these basic techniques in commercial SODAR systems. Very few manufacturers go as far as to extrapolate the wind profiles according to some meteorological model, which depends on the stability classification that is also determined by the SODAR. The big disadvantage of this approach is that model data cannot be distinguished from measured data and therefore data quality cannot be judged. Therefore, this technique is not normally applied.

Every single technique mentioned above has some level of randomness such as the choice of the averaging time or the definition of a maximum level of permitted wind shear. For the future, it is necessary to develop and evaluate a systematic algorithm for both consistency checking and smoothing, allowing for poor data points, and combining several profiles and points within a profile as consistency check resulting not only in the wind profile but also in a general measure of how trustworthy the result is.

2.3.8 Data rejection

Besides data rejection through consistency checks there are other measures for data quality: Signal-to-noise ratio, Number of valid returns within an averaging interval, a measure for clutter that is the strong echo signal from fixed echoes, and vertical wind speed as a measure of scatter from rain.

2.3.8.1 AD-converter overload

For each range gate the incoming signal is tested for overload in the AD-converter. If there is an overload this would have uncontrollable effects on the spectrum, therefore the respective signals are discarded.

2.3.8.2 Signal-to-noise ratio

The signal-to-noise ratio (SNR) is either defined as a ratio of powers or as a ratio of logarithmic powers. It is straightforward to find the SNR below which, the signal is equal to the noise or smaller. Therefore no valid peak can be found and the data point is rejected. However, most systems allow the user to choose a higher SNR thus defining an empirical value when the peak-finding algorithm is supposed to become unreliable and data points are rejected.
To compare the SNRs of different types of SODARs is generally very difficult because of the different ways the noise level is determined. While some systems determine the noise level from every spectrum, others do one or more noise measurements after every pulse or every measurement cycle (three to five beams). Averaging of the noise level of up to several minutes is also common.

2.3.8.3 Clutter flag

If part of the signal is scattered by fixed objects like houses or trees a second strong peak will show up in the frequency spectrum at zero Doppler shift. The peak finding algorithms often mistake this peak for the wind peak. These so called fixed echoes can be detected assuming that the fixed echo does not extend over more than a couple of range gates. Simple vertical consistency checks are normally sufficient to reject fixed echoes.

2.3.8.4 Vertical wind speed

High frequency SODARs are sensitive to the scattering from rain droplets and again the SODAR spectrum is contaminated with a second peak. However, medium to large rain droplets fall with vertical

velocities above the usual atmospheric vertical wind speed of not more than 1 ms^{-1}. Therefore, the peaks can in theory be separated and the real wind speed found. In practice, data points with high vertical wind speeds are often ignored.

2.3.8.5 Number of valid returns within an averaging interval

So far, all data rejection parameters were introduced during spectrum analysis. After this, wind components or vectors are usually averaged over times typically ranging from 1 to 60 min. When a high percentage of data points is missing for a certain averaging interval the reliability suffers and the average value can be rejected. The threshold is mostly chosen empirically.

Kirtzel and Peters 1999 describe additional checks of the spectrum. They also check the spectrum for the minimum power level of the spectrum defining a threshold that should not be exceeded. This is possible because the bandwidth of atmospheric echoes is small in comparison to the bandwidth of the whole spectral width of the FFT spectrum. Kirtzel and Peters reason that only noise or interfering signals can be wide enough to increase the minimum power value of the spectrum.

A last spectral feature used by Kirtzel and Peters is the fact that the spectral width of the signal is known to a certain extend: It cannot be smaller than the width defined by the acoustic beam width, the finite pulse length and the Hanning shaping of the pulse. On the other hand if the spectral width is too large, then the frequency resolution is too poor to give accurate wind speeds. Therefore the threshold is determined by the application.

2.3.9 Wind component calculation uvw

The signal transmitted from a SODAR is a travelling wave with components like $\sin(\omega t - kz)$ or $\cos(\omega t - kz)$ When the wave is scattered at turbulence which is moving with vertical speed w then the returning signal is frequency-shifted due to the Doppler effect. The total Doppler shift is

$$\Delta\omega = -2\mathbf{kw} \,. \qquad \text{(Eq. 10)}$$

If the SODAR beam (Figure 12) is tilted at a zenith angle θ from the vertical, and directed at azimuth angle ϕ with respect to East, and the wind has components $V = (u,v,w)$

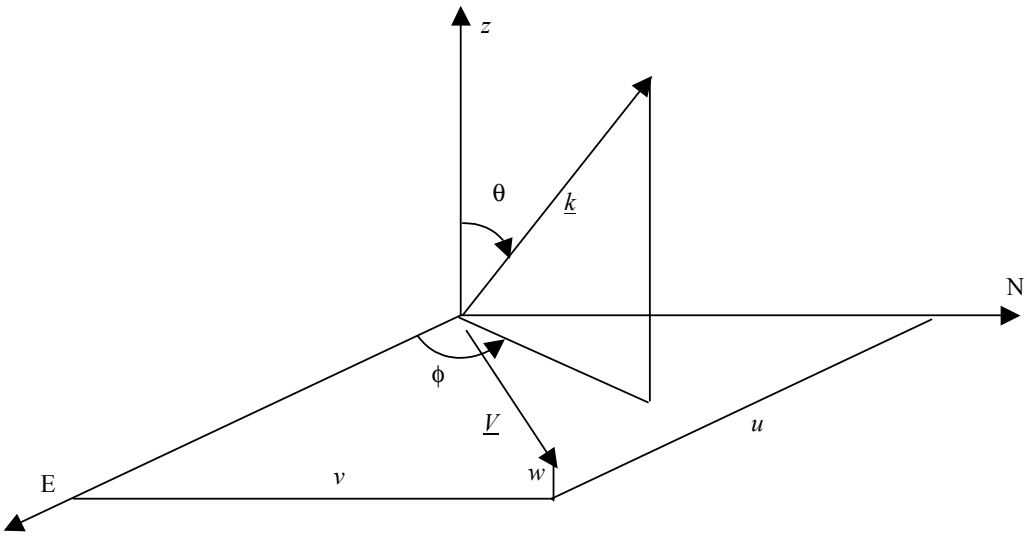

Figure 12 Orientation of the SODAR beams

then

$$\Delta\omega = -2k\left(u\sin\theta\cos\phi + v\sin\theta\sin\phi + w\cos\theta\right) \qquad \text{(Eq. 11)}$$

The *easterly* wind component is u and the *northerly* wind component is v, so an easterly or northerly wind gives a *lower* frequency. Generally SODARs are designed so that they direct two tilted beams in orthogonal planes, say with $\theta_1=\theta_2=\theta_0$, $\phi_1=0$ and $\phi_2=\pi/2$. A third beam is vertical with $\theta_3=0$. Then, at each range gate height, three Doppler shifts are recorded

$$\begin{matrix} \Delta\omega_1 & -2ku\sin\theta_0 - 2kw\cos\theta_0 \\ \Delta\omega_2 & = -2kv\sin\theta_0 - 2kw\cos\theta_0 \\ \Delta\omega_3 & -2kw \end{matrix} . \qquad \text{(Eq. 12 a-c)}$$

Solving for u, v, and w gives the three wind components

$$\begin{matrix} u & -\dfrac{\Delta\omega_1}{2k\sin\theta_0} - \dfrac{w}{\tan\theta_0} \\ v & = -\dfrac{\Delta\omega_2}{2k\sin\theta_0} - \dfrac{w}{\tan\theta_0} \\ w & -\dfrac{\Delta\omega_3}{2k} \end{matrix} \qquad \text{(Eq. 13 a-c)}$$

Since w is usually much smaller than u or v, the w component in the tilted beam Doppler shifts is sometimes simply ignored in calculating u and v. For example, if w = 0.1 m s^{-1}, then for $\theta_0 = \pi/10$ the error in u is 0.3 m s^{-1}. This compares with a typical measurement uncertainty in u of 0.5 m s^{-1}.

Each tilted beam also has finite width $\delta\theta_0$. This causes an extra spectral broadening in the Doppler signal of

$$\frac{\delta\Delta\omega_1}{\Delta\omega_1} = 2\frac{\delta\theta_0}{\tan\theta_0} \qquad \text{(Eq. 14)}$$

(ignoring the w term). Typically $\delta\theta_0 \sim \pm\pi/40$, $\theta_0 \sim \pi/10$, so if k=80 m^{-1} and u=5 m s^{-1}, then $\Delta\omega_1$ =250 rad s^{-1} (Δf_1 = 39 Hz), and $\delta\Delta\omega_1$ =160 rad s^{-1} ($\delta\Delta f_1$ = 26 Hz).

2.3.10 Horizontal wind vector calculation WS, WD

Wind speed WS, and wind direction WD can be directly calculated for each measurement cycle from the wind components:

$$WS = \sqrt{u^2 + v^2} \qquad \text{(Eq. 15)}$$

$$WD = \tan^{-1}\frac{u}{v} \qquad \text{(Eq. 16)}$$

However, the standard deviation of these single shot wind speeds can exceed 1 m s^{-1}due to finite beam width, finite pulse length, Hanning shaping and other effect. This is too large for most applications and therefore averaging is necessary to increase the accuracy.

There are two basic averaging methods: a)Averaging of power spectra before calculating the wind vector and b) calculating the wind vectors, and average wind speed and wind direction separately. The first method gives lower average wind speeds as changes in wind direction result in smaller wind components. The maximum available wind energy can therefore be measured with the second method. Both methods are described below.

2.3.10.1 Averaging of power spectra from successive profiles.

The noise power fluctuates more than the signal, providing the averaging time is not too long (say no longer than 20 minutes, but this signal autocorrelation time will depend on the environment). Noise powers P_{Ni} from the ith profile, at a particular range gate, are summed in the averaging process:

$$\overline{P_N} = \frac{1}{n}\sum_{i=1}^{n} P_{N_i} \qquad \text{(Eq. 17)}$$

and

$$\sigma_{av}^2 = \sum_{i=1}^{n}\left(\frac{\partial \overline{P_N}}{\partial P_{N_i}}\right)^2 \sigma_{P_{N_i}}^2 = \sigma_{P_N}^2 \sum_{i=1}^{n}\left(\frac{1}{n}\right)^2 = \frac{\sigma_{P_N}^2}{n} \qquad \text{(Eq. 18)}$$

so the standard deviation of the noise goes down as the square root of the number of averages.

2.3.10.2 Averaging winds to obtain wind energy

Here we are interested in the wind energy, represented by mean WS^2

We assume there are N measurements u_i, v_i, i=1,2,..,N where the u_i and v_i are measured with individual uncertainties σ_{u_i} and σ_{v_i}. Assume that these uncertainties arise from taking the mean of n_{u_i} values of u, and n_{v_i} values of v, each with variance σ_1^2, so that

$$\sigma_{u_i}^2 = \frac{\sigma_1^2}{n_{u_i}} \qquad \text{(Eq. 19)}$$

$$\sigma_{v_i}^2 = \frac{\sigma_1^2}{n_{v_i}} \qquad \text{(Eq. 20)}$$

where σ_1^2 arises from error in estimating the position of the spectral peak at each range gate, and is essentially the same for each estimation.

Now

$$\begin{aligned}\sigma_{S_i}^2 &= \left(\frac{\partial S_i}{\partial u_i}\right)^2 \sigma_{u_i}^2 + \left(\frac{\partial S_i}{\partial v_i}\right)^2 \sigma_{v_i}^2 \\ &= \left[\frac{1}{n_{u_i}}\left(\frac{u_i}{S_i}\right)^2 + \frac{1}{n_{v_i}}\left(\frac{v_i}{S_i}\right)^2\right]\sigma_1^2 . \\ &= \frac{\sigma_1^2}{\alpha_i}\end{aligned} \qquad \text{(Eq. 21)}$$

is the variance of a single speed S_i , and

$$\sigma_{\theta_i}^2 = \left(\frac{\partial \theta_i}{\partial u_i}\right)^2 \sigma_{u_i}^2 + \left(\frac{\partial \theta_i}{\partial v_i}\right)^2 \sigma_{v_i}^2$$
$$= \left[\frac{1}{n_{u_i}}\left(\frac{v_i}{S_i^2}\right)^2 + \frac{1}{n_{v_i}}\left(\frac{u_i}{S_i^2}\right)^2\right]\sigma_1^2 \qquad \text{(Eq. 22)}$$
$$= \frac{\sigma_1^2}{\beta_i}$$

is the variance of a single direction θ_i.

The mean $\overline{S}$ and $\overline{\theta}$ are required over the N measurements, allowing for the variable uncertainties. These means are found by following the usual procedures for modelling $y = a + bx$, but here we have only one parameter $a = \overline{y}$, so the one-parameter weighted least-squares fit has the form $y = \overline{y}$.
The single parameter, $\overline{y}$, is found by minimizing

$$\chi^2 = \sum_i \left(\frac{y_i - \overline{y}}{\sigma_i}\right)^2 \qquad \text{(Eq. 23)}$$

where σ_i^2 is the variance in measurement y_i, giving

$$\overline{y} = \frac{1}{\sum_i \frac{1}{\sigma_i^2}} \sum_i \frac{y_i}{\sigma_i^2} \qquad \text{(Eq. 24)}$$

and

$$\sigma_{\overline{y}}^2 = \frac{N}{\sum_{i=1}^{N} \frac{1}{\sigma_i^2}}. \qquad \text{(Eq. 25)}$$

In the context of wind-averaging of N=10 one-minute values, this gives

$$\overline{S} = \frac{1}{\sum_{i=1}^{10} \alpha_i} \sum_{i=1}^{10} \alpha_i S_i \qquad \text{(Eq. 26)}$$

and

$$\overline{\theta} = \frac{1}{\sum_{i=1}^{10} \beta_i} \sum_{i=1}^{10} \beta_i \theta_i \qquad \text{(Eq. 27)}$$

where the weights are

$$\alpha_i = \left[\frac{1}{n_{u_i}} \left(\frac{u_i}{S_i} \right)^2 + \frac{1}{n_{v_i}} \left(\frac{v_i}{S_i} \right)^2 \right]^{-1} \quad \text{(Eq. 28)}$$

and

$$\beta_i = \left[\frac{1}{n_{u_i}} \left(\frac{v_i}{S_i^2} \right)^2 + \frac{1}{n_{v_i}} \left(\frac{u_i}{S_i^2} \right)^2 \right]^{-1} . \quad \text{(Eq. 29)}$$

Similar considerations can be used for any other averaged quantities.

An example taken from an AeroVironment 4000 return from 90 m with averaging over 150 s, has measured values of u_i = -3.4 m s^{-1}, σ_{u_i} = 0.8 m s^{-1}, n_{u_i} = 38, v_i=3.7 m s^{-1}, σ_{v_i} =0.9 m s^{-1}, and n_{v_i} =36. This gives S_i =5.0 m s^{-1}, θ_i =313°, and σ_1 =5 m s^{-1}. Then α_i =36 and β_i =920 radian $^{-2}$ m^2 s^{-2}. This means that the standard deviation in wind speed for this averaging period is σ_{S_i} =0.83 m s^{-1} and the standard deviation in wind direction is σ_{θ_i} =9.5°.

2.3.10.3 Wind direction with rotated SODAR

Whereas we have looked at SODARs as being perfectly aligned in North–East orientation so far, SODARs will normally have an input for antenna rotation angle, to allow for an antenna that does not have its tilted beams facing north and east. The SODAR display software, using the following algorithm, should correct for antenna rotation.

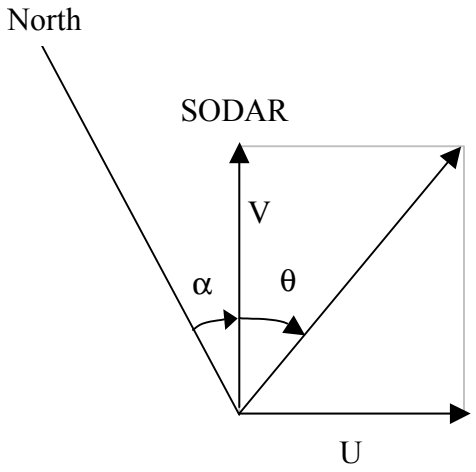

Antenna rotation angle = α

Wind direction : $a + \theta = a + \tan^{-1} U / V$ (Eq. 30a)

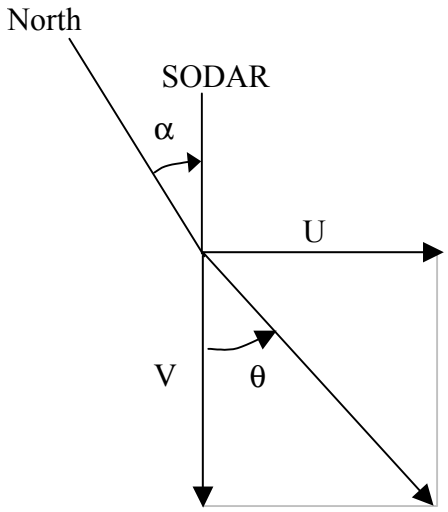

Wind direction = $a + \pi - \tan^{-1} U / V$ (Eq. 30b)

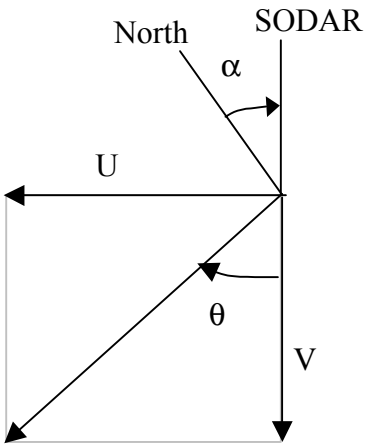

Wind direction = $a + \pi + \tan^{-1} U / V$ (Eq. 30c)

2.4 Conclusions on parameter interdependence

From the descriptions above the conclusion is that some of the variables are affecting each other. For instance, by setting the number of sample points to a higher value also the range resolution of the SODAR is decreased. Therefore the settings of these variables should be decided by taking into account these relations.

The following variables depend on each other:

1. Height resolution Δz_V – pulse length τ – sampling rate f_S– number of sample points N_S

   Range resolution Δz_V = the larger of $\frac{c\tau}{2}$ and $\frac{cN_s}{2f_s}$ (Eqs. 4 and 9)

   Wind speed spectral resolution: Δf_V = the larger of $\frac{f_s}{N_s}$ and $\frac{1}{\tau}$ (Eqs. 31 and 3)

Uncertainty product for winds: $\Delta z_V \Delta f_V = \frac{c}{2}\frac{f_s \tau}{N_s}$ if $f_s \tau > N_s$ (Eq. 32)

$$\Delta z_V \Delta f_V = \frac{c}{2}\frac{N_s}{f_s \tau} \text{ if } f_s \tau < N_s \quad \text{(Eq. 33)}$$

2. Rise time β – effective pulse length $\tau_{eff}(\beta)$?

3. In terms of the power output the effective pulse length changes with the rise time as:
   $\tau_{eff}(\beta) = \tau(1-\beta)$ (Eq. 34)

4. Receive power P_R – pulse length τ

   Via Sodar equation (Eq. 1) $P_R \propto \tau$ (Eq. 2)

5. Range z_{max} – pulse repetition rate T – transmit frequency f_T

There is no simple relation between SODAR range, transmit frequency, and pulse length as the range is determined by the absorption, the turbulence strength and distribution as well as the noise levels. These parameters change with the meteorological conditions and the environmental activity. As a rule of thumb one can assume a range of

$$z_{\max} \approx 2822 \times f_T^{1.76} \quad \text{(Eq. 35)}$$

where the transmit frequency is given in kHz.

This corresponds to a pulse repetition rate of

$$T = \frac{2 z_{\max}}{c} \quad \text{(Eq. 36)}$$

with sound speed c which is also changing slightly with temperature.

When taking these relations into account, the following settings for the AV4000 SODAR is recommended:

Because of these dependencies the following settings are recommended for measurements with Aerovironment SODARs. Other SODARs (METEK, Scintec) should follow this recommendation as close as possible.

Sodar settings		**Advised value**	**Comments**
Met Sampling			
Maximum Altitude	Mht	4000 array = 150 m 3000 array = 250 m	Preventing backscatter from a previous pulse
Altitude Increment	Avdst	4000 array = 10 m 3000 array = 20 m	
Averaging Time	Sec	600 s	In the wise project there will be done some measurements with a averaging time of 60 s. ECN will report about this. There is already a Riso article about this.
Wind Gust detection interval	Ngav	Not important	
Percent acceptable data	Gd	At least 10 %	
W Magnitude Threshold	Wmax	500 cm/s	Should be adjusted in complex terrain
Minimum Altitude	Min Alt	1	
Digital Sampling			
Digital sampling rate	Srate	960	Together with the nfft gives this a range resolution of 22.6 m. The frequency resolution is 15 Hz.
Number of FFT points	Nfft	64	
Signal-to-Noise threshold	Snr	7	Should be 6 to 8
Amplitude threshold	Amp	Not important	This parameter is not important in the cases that the Back parameter is not equal to 0
Adaptive noise threshold	Back	-120	Noise threshold is 120 % of the noise measured after the pulse
Analog bandwidth	Bw	800 Hz	
Clutter rejection	Clut	6	Only clutter rejection on the U and V beams
Noise time constant	Nwt	10 s	
SODAR parameters			
Audio amplitude	Damp	As high as possible	
Pulse length	Pulw	100 ms	Taken into acount the range resolution of 22.6 m which follows from Srate and Nfft and Rise
Pulse transition time	Rise	15 %	Together with Pulw = 100 ms gives this an effective pulse length of 70 ms
DOPPLER Limits			
X axis min radial vel	Mincr	-800 cm/s	
X axis max radial vel	Maxcr	800 cm/s	
Y axis min radial vel	Minbr	-800 cm/s	
Y axis max radial vel	Maxbr	800 cm/s	
Z axis min radial vel	Minar	-400 cm/s	
Z axis max radial vel	Maxar	400 cm/s	
Peak detection limits	Nbini	5	

3. Principal differences between point and volume measurements

The usage of wind energy is essentially the usage of the kinetic energy contained in an atmospheric volume that passes through the rotor plane during a certain time interval. Thus the perfect wind measurement for wind energy purposes would be a plane-integrated wind detection with high temporal resolution. As such measurements are not possible they are usually substituted by point measurements at hub height (often even at lower heights and then extrapolated to hub height) or by volume measurements with remote sensing devices from the ground.

The volume measurements by remote sensing devices (SODAR. LIDAR, RASS, etc.) have a great advantage compared to point measurements in one height: they yield information from different heights simultaneously (tethered balloons would give such data only sequentially). Thus we get a wind profile vertically across the rotor plane. The necessity to vertically interpolate (or even worse extrapolate) wind speed and variance is no longer required.

Therefore, the following text deals with two issues: first we discuss the differences between point and volume measurements (Chapters 3 and 4), and second we investigate the advantages of a profile measurement compared to extrapolations from a point measurement (Chapters 5 and 7).

3.1 Measurement volume

With the emission of one sound pulse, the SODAR detects information (backscatter intensity and radial velocity) from an atmospheric volume with several tens of meters in diameter and about 10 to 20 m in the vertical. Assuming a sound beam width of 8° (3 db-angle, see Figure 13) the diameter of the beam is 14 m at a height of 100 m above ground and 28 m at a height of 200 m above ground. Taking a vertical resolution of 10 m, the measurement volume at 100 m height is about 1540 m³.

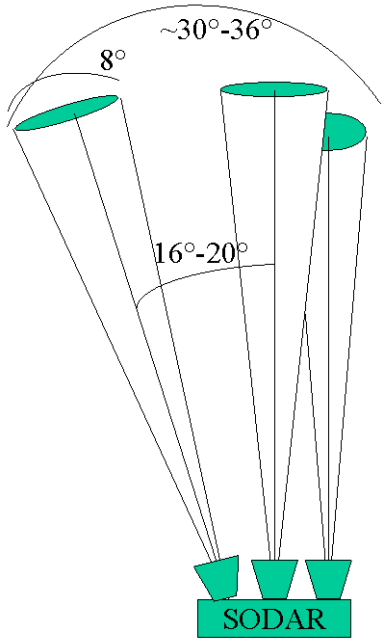

Figure 13. Geometry of SODAR sound lobes

Classical wind measurements with in-situ instruments like cup anemometers (including a wind vane for the measurement of the wind direction), propeller anemometers, or even ultra-sonic anemometers only detect information from a very small volume with a cross-section of about 10 cm radius and a length of a few meters (this is the response distance (MacCready 1966) or the distance constant (Busch and Kristensen 1976) of a usual cup anemometer). This is a volume in the order of 0.1 m³ (i.e. the measurement volume for one radial velocity from a SODAR as defined above is about 20000 times

larger). Therefore, the latter measurements are regarded as point measurements whereas SODAR measurements are regarded as volume measurements.

In order to detect all three components of the wind speed, the SODAR emits sound pulses in three different directions that are typically 16° to 20° apart. One of these is usually the vertical direction. Thus the calculated wind speed from three shots into three different directions is an average over a larger volume resulting to an effective beam width of up to about 36° (see Figure 13). This is equal to a diameter of 73 m at 100 m height or 145 m at 200 m height. Therefore, at 100 m height the effective volume for which the three-dimensional wind vector is determined is about 41850 m³. This is even about 500 000 times larger than the measurement volume of a classical in-situ instrument.

3.2 Data availability

SODAR measurements depend on the state of the atmosphere. If the atmosphere is extremely well mixed, i.e. temperature fluctuations are very small, nearly no sound is reflected from the atmosphere and the signal to noise ratio for the SODAR can be so small that the determination of a wind speed (via the Doppler shift) is not possible (this happens most pronounced in the afternoon during days with strong vertical mixing due to thermal heating, usually days with small mean wind speeds). Further SODAR measurements are disturbed by sound sources in the near vicinity of the instrument (this includes wind noise which is excited at the instrument itself). The latter problem limits the measurement of high wind speeds. Classical in-situ instruments do not depend on the thermal state of the atmosphere, and they are not disturbed by noise.

3.3 Time resolution

In order to reduce the signal to noise ratio SODAR measurements are typically averaged over 10 minutes whereas in-situ instruments (especially ultra-sonic anemometers) yield information with a temporal resolution of down to 0.03 seconds. Cup anemometers have a time resolution τ which depends on the distance constant d of the instrument and the mean wind speed u (Busch and Kristensen 1976).

$$\tau = d / u \qquad \text{(Eq. 37)}$$

With d = 2 m and u = 5 m/s we get τ = 0.4 s. For 10 Hz data we would need τ = 0.05 s or a mean wind speed of 40 m/s. For the derivation of the Weibull parameters typically used for wind power estimation, 10 minutes averages are sufficient.

4. Comparison of wind data from point and volume measurements

First of all, we must state that no way exists to make the information from point and volume measurements directly comparable. Even implying the theory of frozen turbulence would only help to compare an instantaneous line-averaged (parallel to the wind direction) velocity measurement with a time-averaged velocity measurement at one point. A direct comparison would only be possible if a larger number of point measurement devices were distributed equally over the whole volume covered by the remote sensing device. Such an idea is completely unrealistic, even if these instruments could be mounted without disturbing each other.

Therefore, SODAR and point measurements cannot give exactly the same results. Apart from this, there are some additional reasons, why a SODAR should give a different (usually smaller) wind speed than a point measurement by a cup anemometer (a frequently observed feature, see e.g. Crescenti 1997, Reitebuch and Vogt 1998). Crescenti (1997) reviews 20 SODAR comparison experiments from the years 1976 to 1994. He found a mean bias of -0.05 m/s for the SODAR measurements. He found no dependence on the height of the measurements and on the time of the day. Greatest deviations appeared for wind speeds lower than 2 m/s and for wind speeds over 10 m/s. In the latter case (the only relevant case for wind energy use) the deviation can be attributed to ambient noise.

4.1 Fixed echoes

Before judging on the principal deviation between SODAR and other wind speed measurements one should be sure that the SODAR data is not spoiled by fixed-echos from obstacles that are in the same distance from the instrument as the analysed measurement height. Reitebuch (1999) has shown that fixed-echos can be a problem. He found that the bias of a SODAR can depend on the frequency of the emitted sound pulse. The higher the sound frequency was the less was the negative bias. The explanation for this phenomenon is that the sound lobes are focussed the better the higher the frequency is. The width of the sound lobe (3dB-angle, the angle within which the power dcreases to one half) is to a first approximation directly proportional to the wavelength of the emitted sound pulse (Figure 14):

$$\sin\theta_{3db} = 0.514\lambda / D \qquad \text{(Eq. 38)}$$

with the wave length λ of the sound wave and the opening D of the antenna. Also the angle under which secondary lobes appear depends on the sound wave length in a equal manner:

$$\sin\theta_i = (1.64 + 1.02(i-1))\lambda / D \qquad \text{(Eq. 39)}$$

where i is the ordinal number of the secondary lobe.

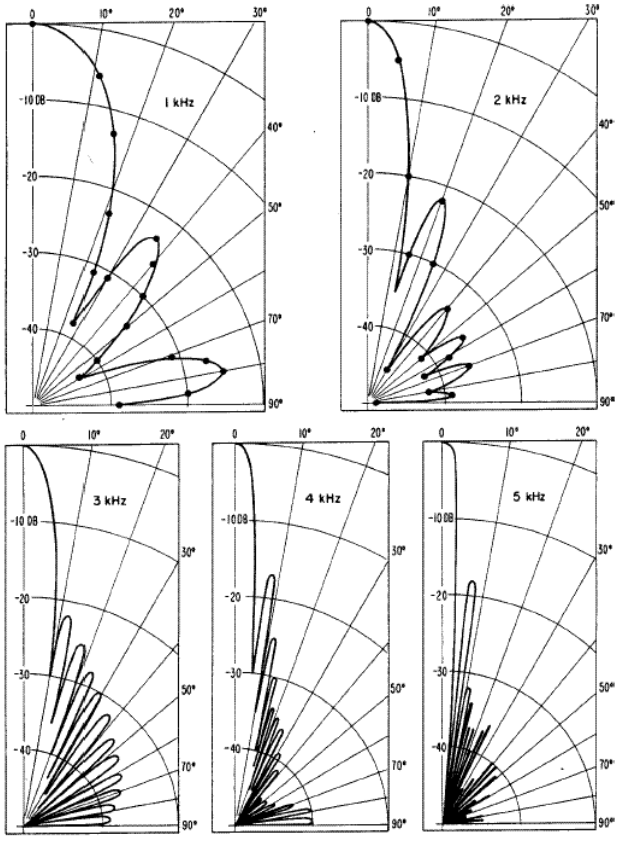

Figure 14 Polar diagrams of the gain pattern of a vertically oriented acoustic beam originating from an unshielded, conical horn reflector acoustic antenna (from Simmons et al., 1971).

4.2 Overspeeding

4.2.1 Definitions

MacCready (1966) has listed four different errors which can appear separately when measuring the wind speed in a turbulent flow: the “u-error”, the “v-error”, the “w-error”, and the “DP-error”. The first three errors appear instantaneously and add up with time. The u-error comes from longitudinal variations in the wind speed (gusts) because a cup anemometer speeds up more rapidly than it speeds

down. The v-error results from azimuthal variations in the wind (wind direction variance), which could lead to misalignments of the measuring device. The w-error is due to turbulent vertical components of the wind, which influence the measurement of the horizontal wind speed. The fourth error, the DP-error appears only when a time average is computed. If there are wind direction fluctuations then the vector average will give a lower wind speed than a scalar average. In order to distinguish between these, the different errors they are dealt with separately in the next subsections.

Comparing our results to results from other sources requires an exact definition of the term 'overspeeding'. Sometimes 'overspeeding' is used only for the u-error, sometimes it is used for all errors together.

The word 'error' for these effects might be misleading, especially for the DP-error. It depends very much on the application for which the mean wind speed has to be determined whether a scalar or a vector average should be formed. If the wrong average is formed then an error is produced.

4.2.2 u-error (longitudinal wind variations, gusts)

Principally, a cup anemometer speeds up more rapidly than it speeds down. This is caused by the fundamental construction, otherwise a cup anemometer would not run at all. Therefore, especially in cases of strong wind fluctuations (large values of the turbulence intensity σ_u/u), a cup anemometer should show a higher mean wind speed. Busch (1965 (cited from Busch and Kristensen (1976)) has shown that the overspeeding is proportional to the square of the horizontal turbulence intensity. MacCready (1966) calls this the 'u-error' and gives a rough estimate of the overspeeding Δu

$$\Delta u \approx 1/20(d/z) \qquad \text{(Eq. 40)}$$

where z is the measurement height and d the distance constant. Busch and Kristensen (1976) derive a more complex relationship, which also takes into account the surface roughness length, and atmospheric stability via the Monin-Obukhov length. An extensive discussion on the biases or errors of a cup anemometer can be found in Kristensen (1993). His estimations for u-error (he calls it u-bias) is less than a few percent that appear under very unstable situations. Westermann (1996) finds independently results (Figure 15) that are close to those of Kristensen.

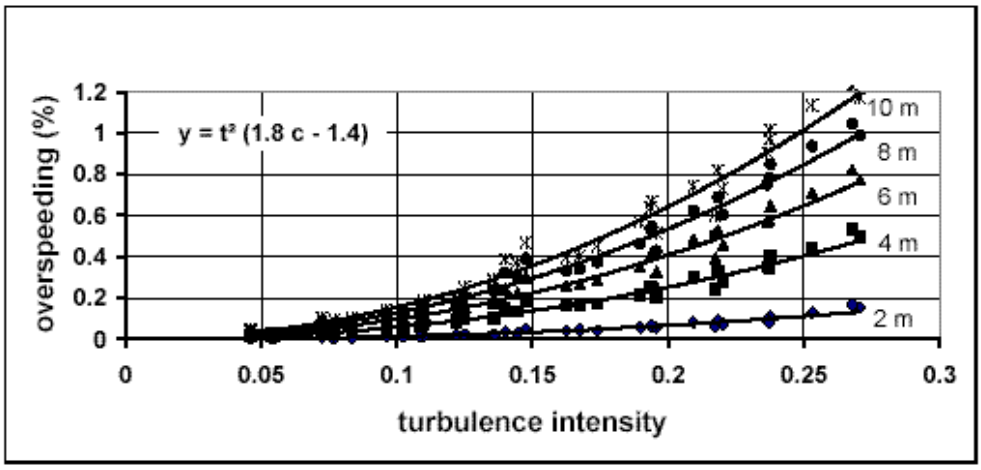

Figure 15 Computed overspeeding y = t² (1,8d - 1,4) with turbulence intensity t and distance constant d (from Westermann (1996))

Kaimal (1986) gives a range of 5% to 10% for overspeeding, especially for convective conditions. As convective situations appear with low wind speeds this might be an indication that overspeeding is larger for lower wind speeds. These wind speeds are not relevant for wind energy purposes.

The problem of the u-error does not appear with propeller and sonic anemometers.

4.2.3 v-error (directional variations in the horizontal)

An error due to lateral wind components ('v-error' in the terminology of MacCready (1966)) is relevant for propeller anemometers only. Therefore it is not discussed here.

4.2.4 w-error (distinction between horizontal and vertical wind components)

A SODAR distinguishes between the horizontal wind components and the vertical wind component. Only the horizontal ones are used when computing the mean wind speed. A cup anemometer is driven not only by horizontal wind components but partially also by the vertical wind component (see e.g. Albers et al. 2002). This error is called 'w-error' by MacCready (1966) and increases with unstable atmospheric stratification. According to MacCready an overestimation of the horizontal wind speed by 10% is probably not uncommon.

Figure 16 shows an evaluation of data from an ultrasonic anemometer at 50 m above ground which have been taken under nearly neutral thermal conditions over flat terrain. The mean horizontal wind speed was just above 7 m/s, the mean vertical component of the wind speed was zero. One minute averages of these sonic data have been processed in two ways: once only the horizontal wind components have been used for the determination of the hourly mean wind speed (2D), and in a second evaluation all three components have been used (3D). The ratio of these two wind speeds have been plotted against the 3d turbulence intensity. For a turbulence intensity of 25% this error comes close to 1%.

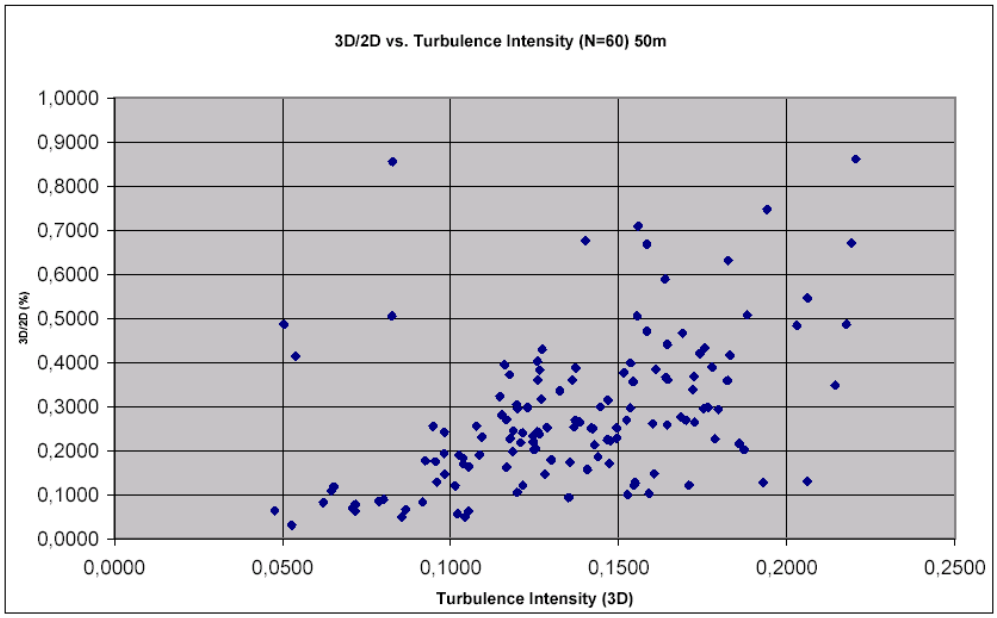

Figure 16 Simulated w-error from sonic data plotted against turbulence intensity.

4.2.5 DP-error (time averaging)

A cup anemometer measures continuously and averages the wind speed regardless from which direction the wind is coming. A SODAR performs short measurements of 100 to 150 ms every four seconds (in case of a mini-SODAR with a height range of 150 to 200 m) and calculates from these discontinuous data a vector mean, i.e. it averages the three wind components before computing the wind speed. In cases of varying directions (e.g. in the presence of turbulence) a vector mean is smaller than a scalar mean. This error is called 'DP-error' (data processing error) by MacCready (1966) and can reach 10% of the mean speed if the variance of the wind direction is greater than 30° (which is not uncommon for MacCready).

The same data set that has been used to derive the values shown in Figure 16, has been used also to simulate the dependence of the DP-error on the turbulence intensity. The result is shown in Figure 17. For a turbulence intensity of 25% we find a DP-error of about 2.5%. The DP-error is is addressed theoretically in more detail in Chapter 6.

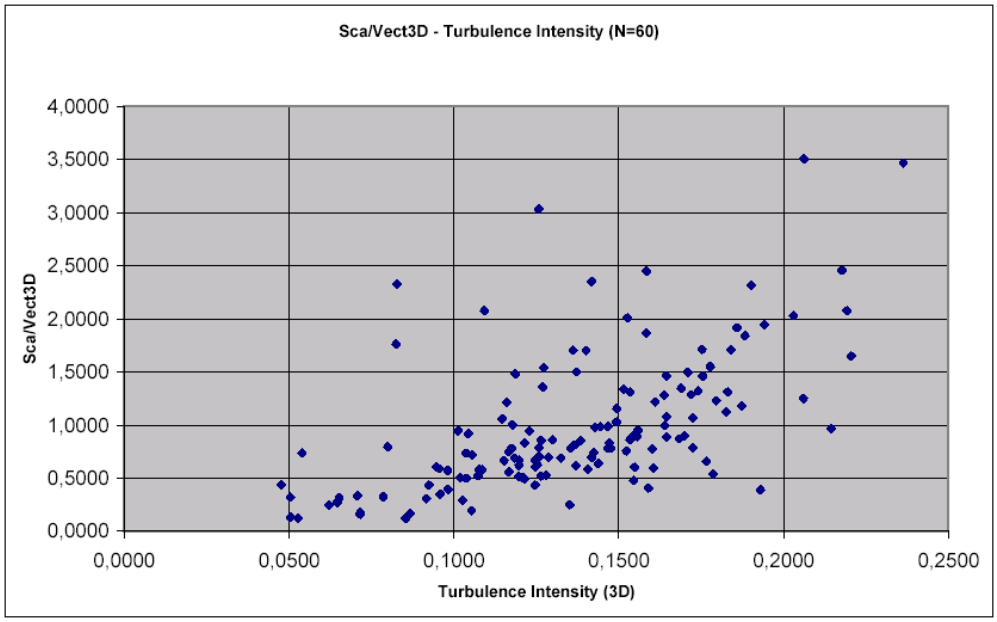

Figure 17 Simulated DP-error from sonic data plotted against turbulence intensity.

4.2.6 Summary of errors

Comparing cup anemometer and sodar measurements all three errors should appear together. Having 1% from the u-error, 1% from the w-error, and 2.5% from the DP-error, we expect a sodar to measure about 4.5% less than a cup anemometer.

5. Principal differences between point and profile measurements

The SODAR (as other ranging remote sensing devices like RADAR and LIDAR) yields nearly simultaneous information from a height range (typically up to a few hundred meters above ground) whereas classical in-situ instruments only yield information for one height.

This offers two advantages: first, a measurement directly in hub height is possible and no extrapolation from a point measurement at a somewhat lower mast is necessary. Extrapolation of point measurements to other heights enters unwanted uncertainties into the wind determination in the rotor plane (see Chapter 5.1). Second, assumed a point value for hub height is available, this value must not be taken constant over the rotor plane but the wind power estimation can be done with the measured vertical profile across the rotor plane (see Chapter 5.2).

5.1 Errors due to vertical extrapolation of wind and variance data

5.1.1 Mean wind speed and scale factor of Weibull distribution

The usual vertical extrapolation for mean wind speed (and alike for the scale factor of the Weibull distribution) with the logarithmic law or a power law is applicable in the Prandtl layer only. The top of the Prandtl layer which roughly forms the lower 10% of the atmospheric boundary layer is somewhere between 60 and 80 m above ground.

In the Prandtl layer the impact of the Coriolis force is negligible, and the vertical wind speed profiles are usually described by the logarithmic profile and the respective correction functions (Businger et al. 1971, Dyer 1974) for the thermal stratification of this layer. In engineering applications these profiles are often approximated by a more simple power law (Davenport 1965):

$$u(z) = u(z_A) \bullet (z / z_A)^n \qquad \text{(Eq. 41)}$$

where z_A is the height of the available measurements and n is an empirical factor which comprises the influences of both surface roughness and atmospheric stability. n increases with increasing surface roughness and with increasing thermal stability of the surface layer.

Above the Prandtl layer in the Ekman layer the Coriolis force additionally influences the shape of the wind speed profiles. Here the following analytical expression for the vertical profile of the wind speed can be derived if a vertically constant coefficient of the turbulent vertical exchange of momentum K_M is assumed (e.g. see Stull 1988):

$$u^2(z) = u_g^2(1 - 2\exp(-\gamma z)\cos(\gamma z) + \exp(-2\gamma z)) \qquad \text{(Eq. 42)}$$

with
- γ^2 $f/2K_M$ (f is the Coriolis parameter, K_M the vertical mean of the coefficient of turbulent vertical exchange of momentum), and
- u_g the geostrophic wind speed.
- π/γ is a measure for the vertical depth of the Ekman layer
- γ is via K_M a function of the thermal stratification of the atmosphere as well as of the roughness of the orography.

As γ is determined by orography also it is a site-specific parameter which is principally unknown and which can only be gained from measurements made at the foreseen site. Therefore Eq. 42 (and later Eq. 44), still contain a source of error when used for the vertical extrapolation of mean wind speed and the scale factor of the Weibull distribution, albeit both are much more suited for wind turbines with high hub heights than Eq.41.

If γ is small, i.e. when the thermal stratification of the air is unstable and γ is in the order of 10^{-3} m^{-1}, Eq.42 can be even more simplified (Emeis 2001). If z is small compared to $1/\gamma$ then the cosine-function in Eq. 42 is close to unity. So we get in this case:

$$u^2(z) = u_g^2(1 - 2\exp(-\gamma z) + \exp(-2\gamma z)) \qquad \text{(Eq. 43)}$$

and after taking the square root we end with:

$$u(z) = u_g(1 - \exp(-\gamma z)) \qquad \text{(Eq. 44)}$$

Eq. 42 or Eq. 44 can be used for the approximation of measured vertical wind profiles and of vertical profiles of the Weibull scale factor A. Eq. 42 is the physically correct equation, Eq. 44 is a more simpler approximation to Eq. 42. A fit to the measured values with Eq. 42 or Eq. 44 instead of Eq. 41, is easier because two tuneable parameters (u_g and γ) are available. In contrast to Eq. 41, Eq. 42 and Eq. 44 are not coupled to a measured value in a certain height but only to the asymptotic value u_g which is met in larger heights. u_g is the geostrophic wind speed that is approximately equal to the gradient wind speed, which is approached asymptotically by the wind profile with increasing height above ground. $1/\gamma$ in the simplified equation Eq. 44 is the height above ground in which 63.2% of the asymptotic value is reached ($(u_g - u)/u_g$ is equal to 1/e).

The Figure 18 and Figure 19 (taken from Emeis 2001) demonstrate the possible errors and show the differences between the vertical profiles expressed by Eq. 41) and Eq. 44 and make a comparison to measured wind profiles for flat terrain and for hilly terrain. Figure 18 displays the vertical profiles of the Weibull scale factor for three 30 day periods in 1999 over nearly level terrain. Whereas May 1999 and especially April 1999 were characterized by low mean wind speeds and a large number of days with local thermal forcing of the boundary layer, the chosen 30 day-period from autumn was dominated by stronger larger-scale winds. Also shown is the mean profile for the five 30 day periods April to July and autumn.

Because higher wind speeds are much more important for wind energy production (the production is proportional to the third power of the scale factor, we have tried to fit the analytical profiles from Eq. 41 and Eq. 44 to the autumn curve. As the scale factor of the Weibull distribution is principally proportional to the mean wind speed we use Eq. 41 and Eq. 44 by putting the scale factor A(z) instead of the mean wind speed u(z), and A_g instead of u_g. A bundle of curves computed with exponents n varying between 0.15 and 0.30 has been adapted to the measured scale factor $A(z_A)$ at z_A = 30 m a.g.l. Obviously, the curve for n = 0.30 describes the vertical profil of the scale factor A(z) quite well for heights below 60 to 70 m. Above this height the scale factor extrapolated by Eq. 41 becomes larger than the observed profile. Above heights of about 50 m a curve computed from Eq.44) with A_g = 6.98 ms^{-1} and γ = 0.030 m^{-1} describes the measured data very well. This fact is not very surprising because Eq. 41 has been derived from surface layer data, and Eq. 44) has been derived from Ekman layer principles. As the validity of the power law in Eq. 41 is a typical feature of the surface layer we can assume that at this site in autumn the top of the surface layer was at about 60 m. For comparison the climatological wind profile from WAsP is also given in Figure 18. It shows a constant increase of the wind speed with height, which is in some contradiction to theoretical considerations (Eq. 41 and Eq. 44) and to the findings in Manier and Benesch (1977).

Figure 19 shows a comparable graph as Figure 18 for the hill top site in the Saarland. Again a bundle of curves computed from (Eq. 41) with exponents n varying between 0.25 and 0.40 has been adapted to the measured scale factor $A(z_A)$ at z_A = 30 m a.g.l. This time the power law (Eq. 41) is not at all suitable for the description of the vertical profile of the scale factor. Again, above heights of about 50 m a curve computed from Eq. 44) with A_g = 10.67 $ms^{-1}$and γ = 0.035 m^{-1} describes the measured data very well. Also the deviation between the two curves below 50 m is much lower than in Figure 18 This indicates that the whole wind profile over hill tops is much better described by Ekman layer dynamics than by surface layer dynamics, which again could have been expected. Once again the curve from WAsP is added. This time, the Wind Atlas programme gives too low wind speeds. No real difference can be found between the vertical profiles of the scale factor from WAsP for level terrain and for the hill top site. This fact is reproduced in the wind data (Traup and Kruse 1996) for the stations Deuselbach and Lüchow, which are both not very far from the sodar measurement sites, used here.

Note that fitting a measured wind profile with Eq. 42 and with Eq. 44 leads to two different values for γ which influences the curvature of the fitted vertical profile. Table 1 demonstrates the differences between the two approximations . The maximum deviation that is given in the rightmost column of this table occurs close to the ground (in the table computed for 25 m above ground). The strong increase of the deviation between Eq. 42 and Eq. 44 with increasingly stable stratification demonstrates clearly that the simpler form should only be used for unstable stratification (at least as long as γ should remain a interpretable quantity).

Table 1 Values for the parameter γ in the equations (42) and (44), assuming a Coriolis parameter f = 0.0001 and that the wind speed profiles have identical values at 150 m above ground. The column 'deviation' gives the maximum deviation between the two proflies from (42) and (44) in the first 300 m above ground

Stratification of the air	Coefficient, turb. exchange in m^2/s	Eq. 42 γ in m^{-1}	Ekman layer. depth π/γ in m	Eq. 44 γ in m^{-1}	Deviation bet eq. 42 and eq. 44 in %
unstable	100	0,000707	4488	0,001023	2
neutral	10	0,002236	1428	0,003420	7
stable	1	0,007071	442	0,014400	32

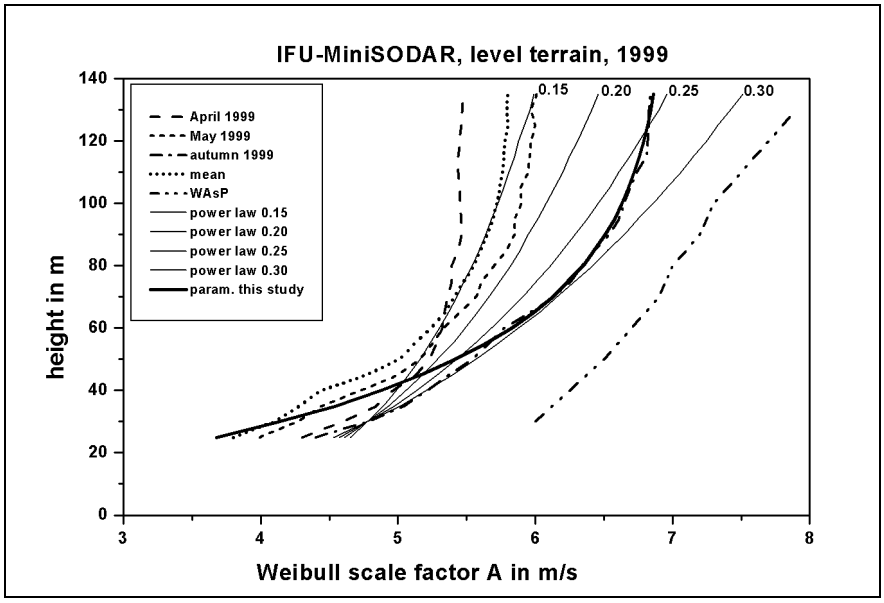

Figure 18 Measured (by a mini-SODAR) and parameterised (see text) vertical profiles of the scale factor of the Weibull distribution over flat terrain (taken from Emeis (2001)).

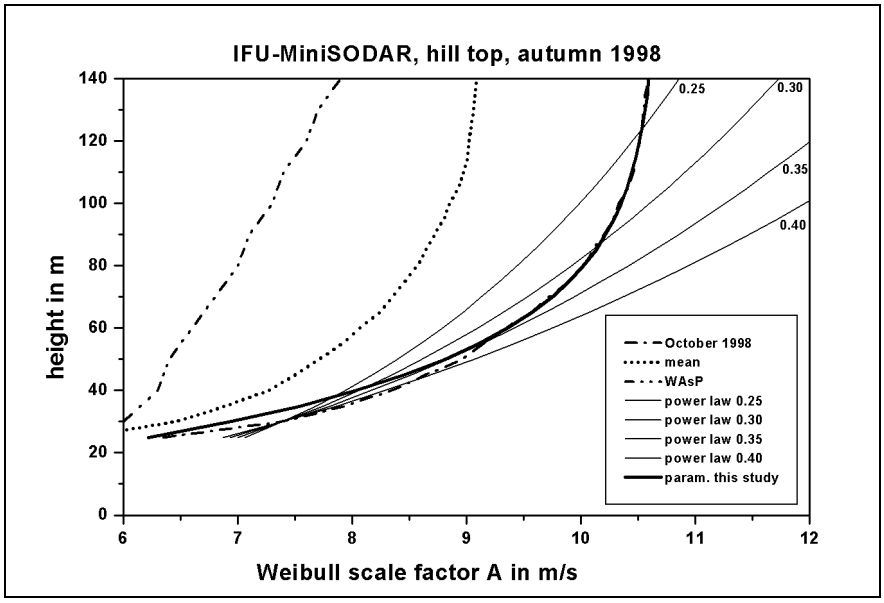

Figure 19 Measured (by a mini-SODAR) and parameterised (see text) vertical profiles of the scale factor of the Weibull distribution over a hill top (taken from Emeis (2001)).

5.1.2 Wind variance and form factor of Weibull distribution

The usually assumed increase of the form factor of the Weibull distribution with height is also applicable for the Prandtl layer only. In contrast to the theoretically derived profiles for the mean wind speed (Eq. 41 and Eq. 44), in recent years several empirically derived profiles have been proposed for the low-frequency variance of wind speed and the shape parameter k of the Weibull distribution. Justus et al. (1978) fitted profile functions from tower data up to 100 m a.g.l. by:

$$k(z) = k_A(1 - c\ln(z_A / z_{ref}))/(1 - c\ln(z / z_{ref})) \qquad \text{(Eq. 45)}$$

with k_A as the measured shape parameter in the height z_A, z_{ref} = 10 m, and c = 0.088. As 100 m a.g.l. may already be above the expected maximum in the k-profile at the top of the surface layer, the overall slope of k(z) below this maximum might be underestimated if Eq. 45 is used. Justus et al. were principally aware of the existence of a maximum in the k-profile but assumed that this maximum would

occur in heights above 100 m. Later Allnoch (1992) proposed to put c = 0.19 and z_{ref} = 18 m in order to better represent the slope of the k-profile below its maximum at the top of the surface layer.

But the form factor has a maximum at the top of the Prandtl layer and decreases again above this layer. The form factor is inversely proportional to the daily variation of the wind speed. In the Prandtl layer wind speed is highest around noon and lowest in the night. At the top of the Prandtl layer this variation nearly vanishes. Above the Prandtl layer the wind speed tends to be higher at nighttime than at daytime. Therefore, the daily variation of the wind speed is lowest at the top of the Prandt layer. Inversely, the form factor has its maximum there. An interpolation formula for the form factor, which takes this vertical variation into account, is available from Wieringa (1989). He rather parameterises the difference $k(z) - k_A$ instead of the ratio $k(z)/k_A$ by putting:

$$k(z) - k_A = c_2 (z - z_A) \exp(-(z - z_A)/(z_m - z_A)) \qquad \text{(Eq. 46)}$$

with the height of the maximum of the k-profile z_m, and a scaling factor c_2 of the order of 0.022 for level terrain. c_2 determines the range between the maximum value of k(z) at height z_m and the asymptotic value of k at large heights. We can use Eq. 46 for the approximation of measured data.

As in Eq. 44 for the approximation of the mean profiles we have in Eq. 46 two tuneable site-specific parameters which have to be determined from experimental data. As long as they are not known exactly they are a source of error when used for vertical extrapolation. The possible errors are demonstrated in Figure 20 and Figure 21 (again taken from Emeis 2001).

Figure 20 shows vertical profiles of k(z) for several months and for a mean over five months over nearly level terrain. In all curves we find a maximum between 50 and 80 m above ground. As in Figure 18 we try different fittings to the autumn curve. Here we apply the empirical schemes from Eq. 45 and Eq. 46. Eq. 45 needs three input parameters: the measured value of k at the height z_A, and the two parameters z_{ref} and c. Eq. 45 is – as it has been designed – not able to reproduce the maximum of k(z) but rather produces monotonically rising curves. Neither the proposed values for the two free parameters by Justus et al. nor the values proposed by Allnoch yield curves which are close to the observed ones. Eq. 46 proposed by Wieringa works much better. Using the observed value of k at height z_A, and the two parameters z_m = 75 m and c_2 = 0.06 we get the thick curve in Figure 20, which fits quite well to the observed curve for October, and which reproduces the maximum in the profiles. The climatological k-profile computed with WAsP for this site does not reproduce the maximum in the profile and is quite close to the result from Eq. 45 when using the constants proposed by Justus.

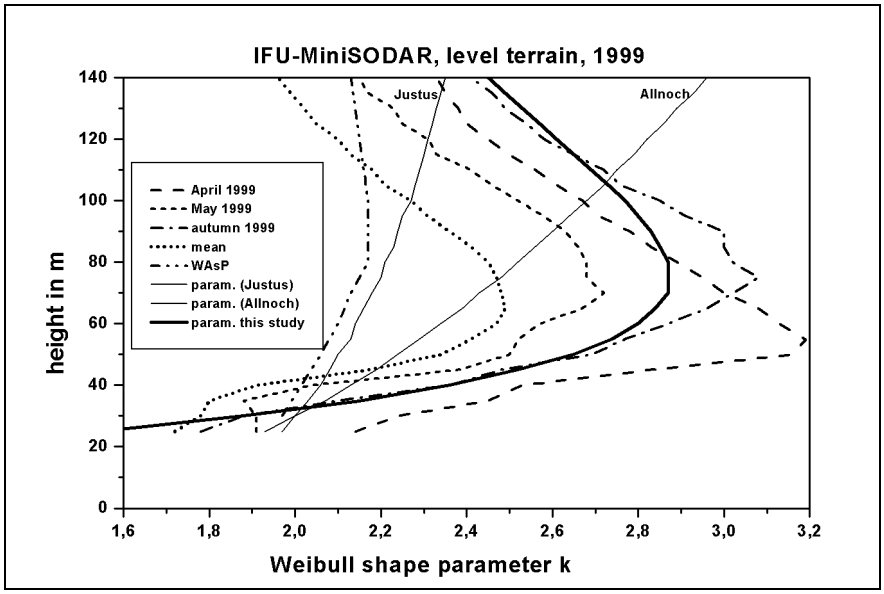

Figure 20 Measured (by a mini-SODAR) and parameterised (see text) vertical profiles of the form factor of the Weibull distribution over flat terrain (taken from Emeis (2001)).

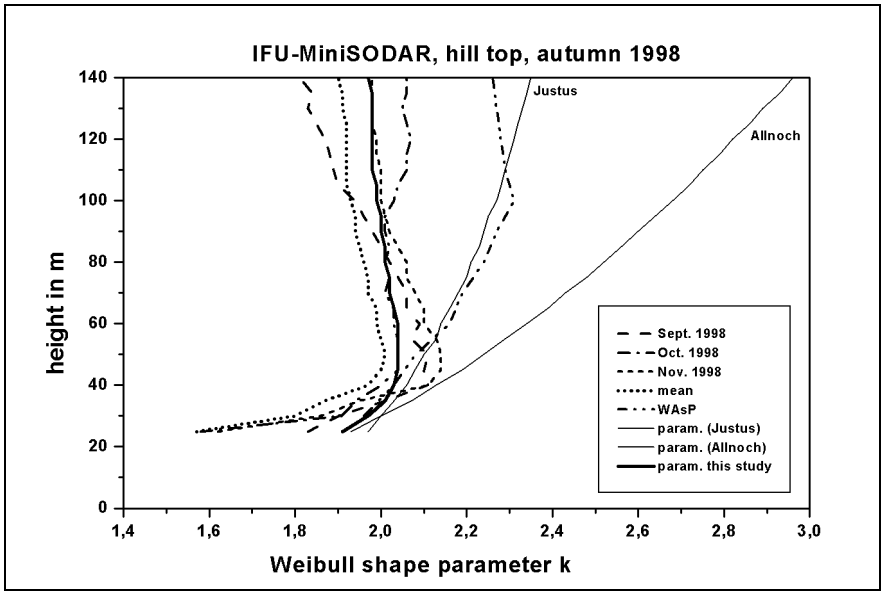

Figure 21 Measured (by a mini-SODAR) and parameterised (see text) vertical profiles of the scale factor of the Weibull distribution over a hill top (taken from Emeis (2001)).

Figure 21 presents k-profiles for the hill top site. Again, the measured k-profiles show a maximum around 50 m above ground, although it is not as clear and pronounced as the maximum in the k-profiles over level terrain. All in all the variation with height is much less than over level terrain. The parameterised k-profiles from Eq. 45 are the same as in Figure 20. This time, the slopes of these profiles fit better to the observed slopes below the maximum in the k-profiles. Especially the parameters proposed by Allnoch fit quite well for heights below 50 m a.g.l. But once again, the Eq. 46 can only describe the behaviour of the curves above the maximum. Here the parameters z_m = 50 m and c_2 = 0.01 have been used to produce the curve which fits to the October curve. For a fit to the September and November curves a value of c_2 = 0.03 would be more appropriate. Again, the climatological profile from WAsP is quite close to the profile computed from Justus' proposals. The height of the slight maximum in the WAsP-curve is far too high.

5.2 Errors due to the assumption of constant wind speed over the rotor plane

5.2.1 Errors in mean wind speed

If the increase of wind speed with height across the rotor plane is non-linear (e.g. logarithmic or exponential) the true wind profile should give an average along the vertical, which is different from an average that is based on a constant wind speed at hub height.

Figure 23 gives an example for this generally small difference. Due to the decreasing curvature of the mean wind speed profile with height the deviation depends on the hub height and the rotor diameter. The example is based on a logarithmic wind profile for a roughness length of 0.5 m and a friction velocity of 0.7 m s^{-1}. It is further assumed that the lifting force is constant along the longitudinal axis of the blades. In reality the lifting force varies with wind speed in different ways depending whether the wind turbine is stall- or pitch-regulated. In a pitch regulated wind turbine the whole blade is turned 90 degrees along the axis in case of too high wind speeds, in a stall regulated wind turbine the blade is only turned so far that the laminar flow around the blade stops. Close to the blade tips and very near to the rotor axis the lifting force decreases in any case, Figure 22.

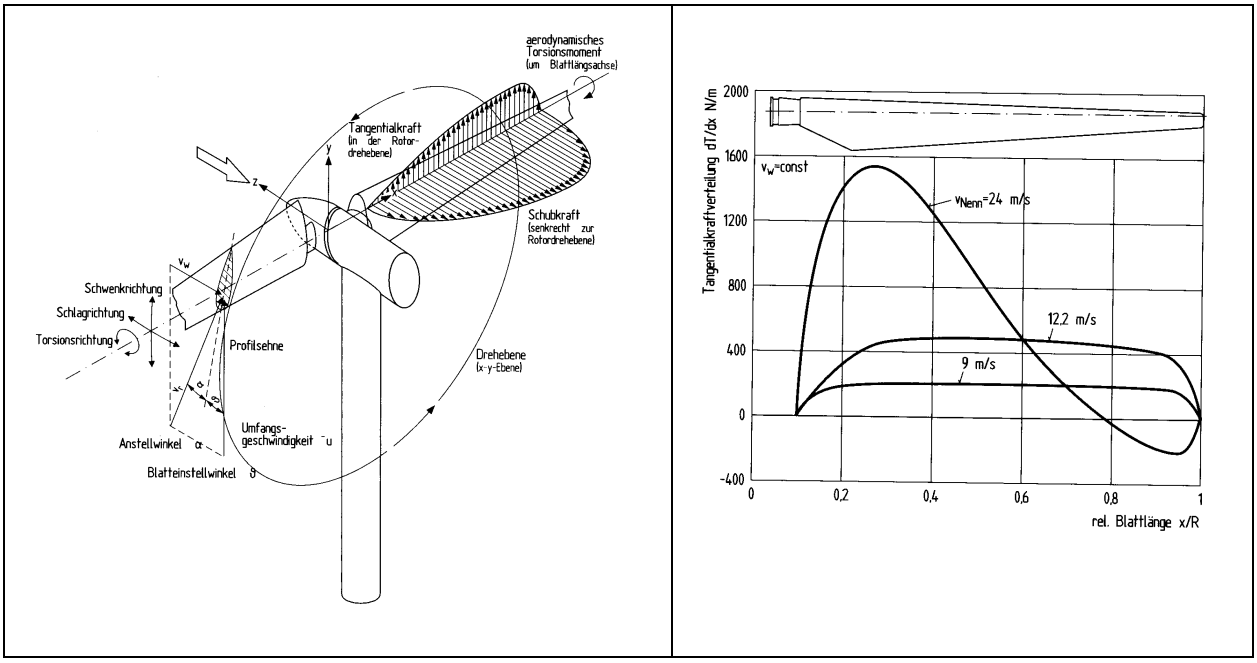

Figure 22 Lifting (tangential) force along a rotor blade (left: stall regulated wind turbine, right: pitch regulated wind turbine) (From: Hau 2002)

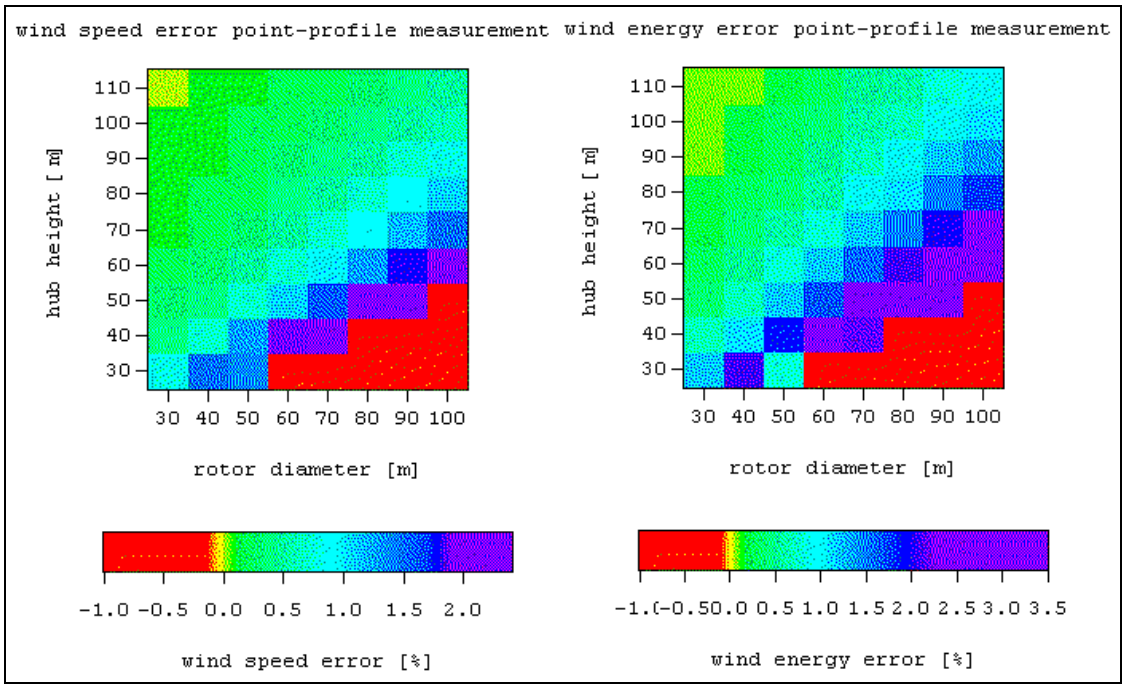

Figure 23 Overestimation of wind speed (left) and available wind energy (right) as a function of hub height and rotor diameter in % when using point measurement of wind speed at hub height instead of using a wind profile measurement by SODAR. Red area in the lower right corner: no data.

It turns out that the error in wind speed is not larger than 2% and the error in wind energy is not larger than 3.5%. The reason that the error in the available wind energy is not about three times the error in wind speed is due to the smaller curvature of the wind energy profile compared to the wind speed profile (see Figure 24). When integrating vertically over the wind and wind energy profiles the area of the rotor plane in the respective height has been considered, i.e. the centre of the rotor plane contributes much more to the integral than the upper and lower edges.

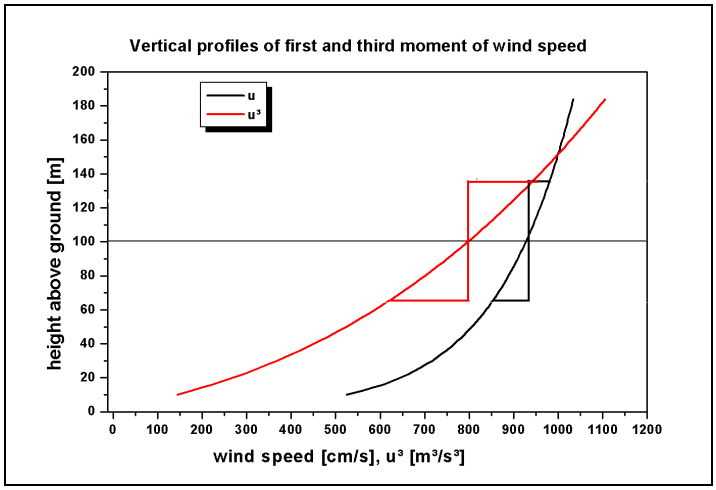

Figure 24 Vertical profiles of mean wind speed and available wind energy

5.2.2 Consequences due to the wind speed difference between the lower and the upper rotor part

The knowledge of the wind speed all over the rotor of a turbine is also important for the following reason: Alternating loads on blades due to the non-uniform wind profile lead to fatigue of the structures and unwanted forces on the axis. The maximum difference between wind speeds at the lower and the upper part of the rotor can be expected in flat terrain during clear nights during the occurence of low level jets (LLJ). A typical example of a LLJ has been observed by a Sodar on October 19, 2001 over Hannover in Northern Germany (Figure 25). On mountain tops the difference between the wind speed between the lower and the upper blade tips is lower than over flat terrain because the strongest wind speed increase is there in much lower heights.

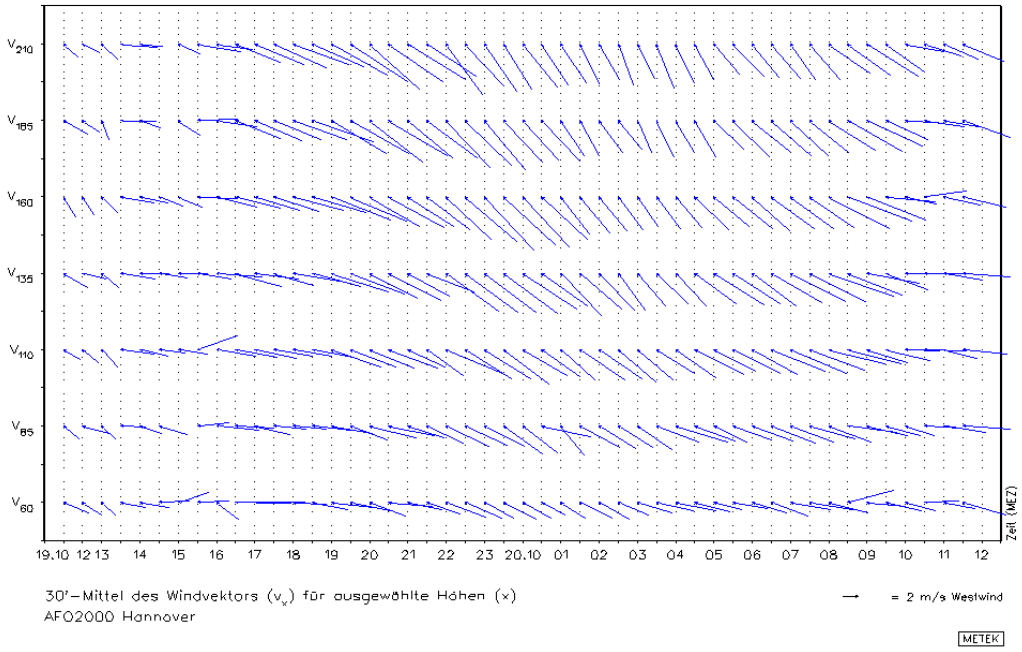

Figure 25 Low-level-jet over Hannover (Northern Germany) in the night form October 19 to 20, 2001 observed by the METEK DSDR3x7 SODAR. The arrows depict horizontal wind direction (orientation) and speed (length, scale to the lower right of the figure).

Profile measurements of wind speed could lead to two additional design factors for the characterisation of sites for wind turbines: a relative vertical difference in the mean wind speed between the lower and the upper tip of the rotor plane and a relative vertical wind speed difference over this plane for a selected 10 minutes average which occurs with a certain probability. Figure 26 shows how these two parameters vary with hub height and rotor plane diameter. The left-hand frame in Figure 26 has been computed from the wind profile given in Figure 24 and by the full line in Figure 27.

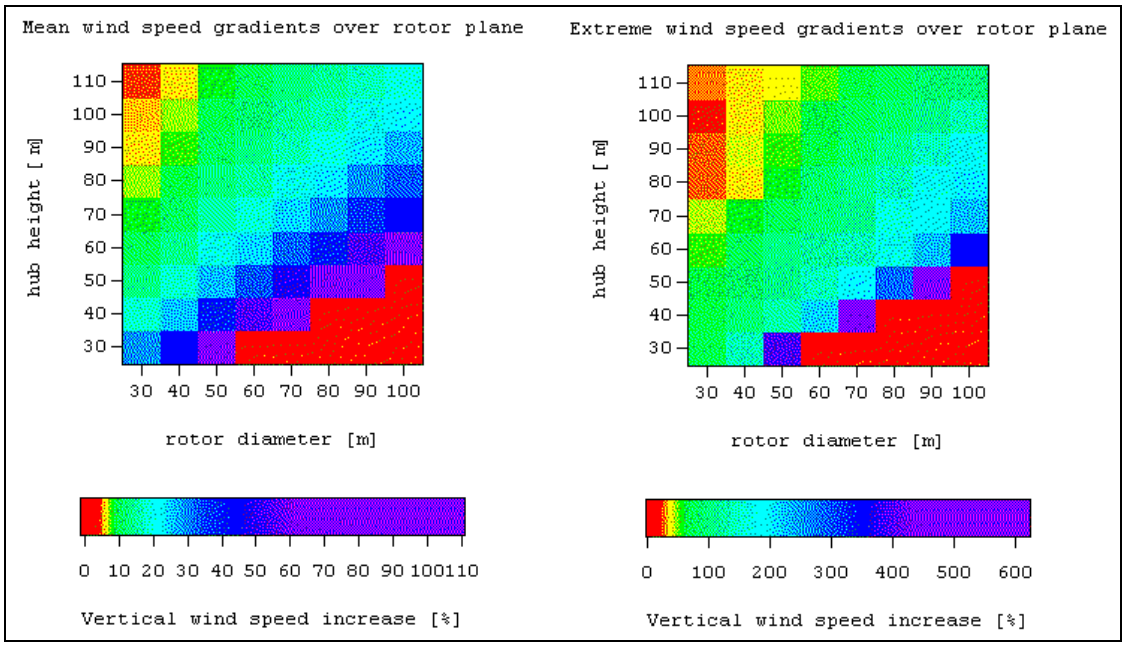

Figure 26 Vertical gradient of mean wind speed (left) and extreme case (October 19, 2001, right) as a function of hub height and rotor diameter in % derived from measurements by SODAR. Red area in the lower right corner: no data. The wind profiles are given in Fig. 27.

For large rotor diameters and low hub heights the mean wind speed at the top of the rotor plane can be about double as large as at the lower edge, especially at night-time. In extreme cases (the right frame of Figure 26 shows a half-hour average measured from October 19, 2001 at 2300 hours CET over Hannover (Northern Germany)) the wind speed could be five times as large. At that night a low-level-jet appeared over Hannover with the jet axis at 160 m above ground. Maximum jet speed was about 10 m/s (see dashed curve in Figure 27). A situation which lasted for several hours and which appears in about 10% of all nights over Northern Germany (Kottmeier et al. 1983). The height of the wind speed maximum usually varies between 100 and 500 m. Therefore the plot to the right displays the most drastic case having the jet axis just in the height of the upper blade tip for a turbine with 110 m hub height and 50 m rotor radius.

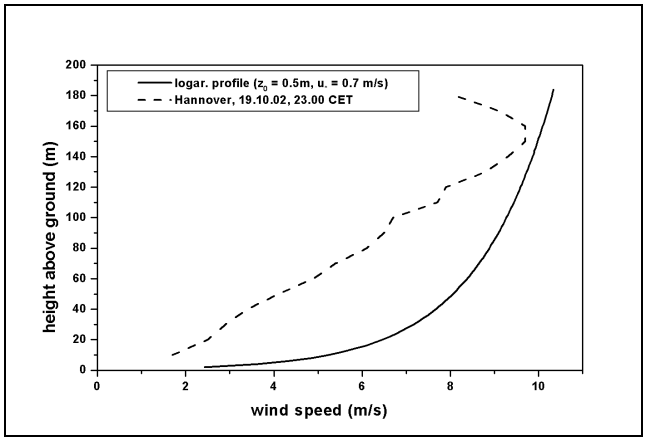

Figure 27 Wind profiles used in Fig. 26 left (dashed curve) and in Fig.26 right (full curve).

A single LLJ event usually covers a large area of several hundreds of kilometers in both length and width. Thus it can happen at the same time in the whole area between Poland and the Dutch North Sea coast, and between Denmark and the middle of Germany (see e.g. Fig. 10 in Corsmeier et al. 1997). LLJs have been observed in many parts of the world. Wippermann (1973) cited reports on LLJs from USA, Canada, West-Peru, Sahara, Kenya, Tropical Africa, the Sovjet-Union, the Indian Ocean, and the Antarctic Plateau. The time of the occurence of the wind maximum is a function of geographical latitude: the farer south the later. Wippermann (1973) presents the following table:

φ	50°	40°	30°	20°	10°
local time of maximum	22	23	01	05	09

LLJs are more pronounced over flat terrain because they can best develop at the top of undisturbed horizontally homogeneous boundary layers.

But there is another reason why strong wind speed gradients over the rotor plane are more likely in flat terrain then over hill tops. Over hill tops we find the phenomenon of speed-up. I.e., the wind speed at a given height above ground is higher over the hill than over flat terrain. Therefore the strongest vertical increase in wind speed over hill tops is in the lowest layers. Here the vertical increase is larger than over flat terrain. The height of the maximum speed-up depends on the hill size and shape. It is usually found in several tens of meters above ground. Above the height of maximal speed-up the vertical increase in wind speed over hill tops is lower than over flat terrain. The typical difference between vertical wind profiles over flat terrain and hill tops is depicted in Figure 28. The assumed hill has a half width of 200 m and a height of 40 m. In Figure 28 no LLJs have been considered, that lead to larger vertical gradients. E.g., SODAR-measurements over flat terrain in Northern Germany yielded an average vertical wind speed increase between 80 m and 125 m above ground of about 20%, whereas the increase over a hill top in the same height range was found to be only about 10%.

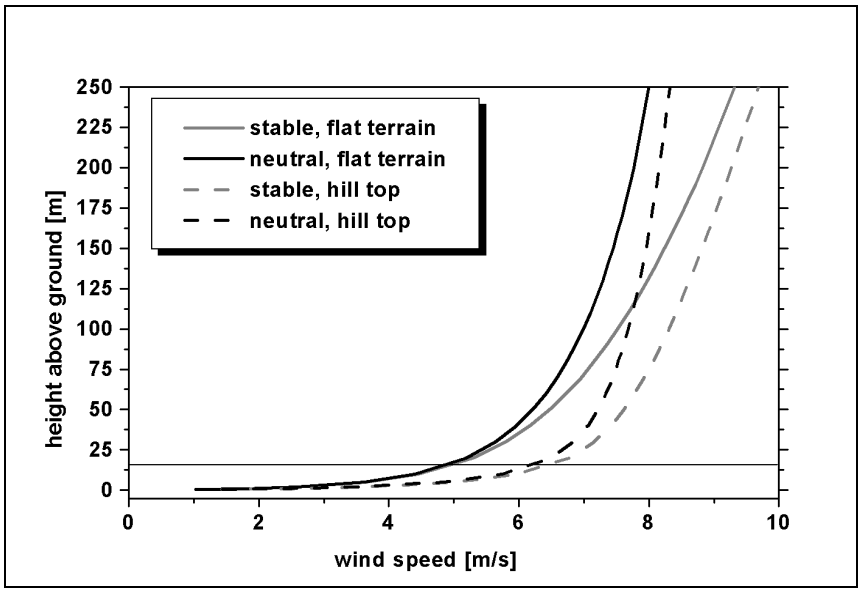

Figure 28 Vertical wind profiles over flat terrain (full lines) and over a hill top (dashed lines) for neutral (black curves) and stable (grey curves) stratification ($L_* = 1000$), a roughness length of 0.2 m and a friction velocity of 0.45 m/s. The height of the inner layer (i.e. the height of maximum speed-up) is about 15 m (thin horizontal line).

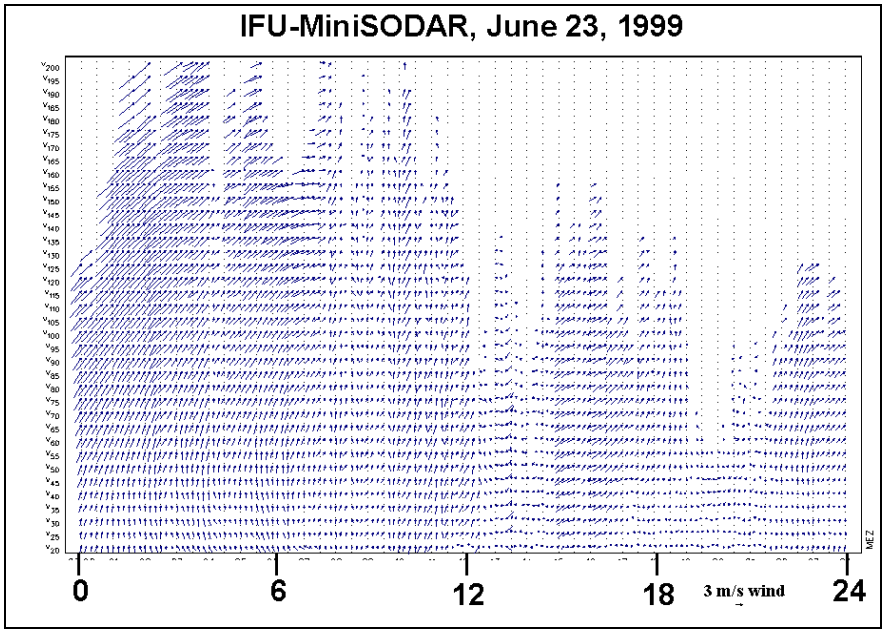

Figure 29 Observed case of extreme directional wind shear on June 23, 1999 over A foreseen wind power site in Northern Germany observed by the Aerovironment AV4000 Mini-SODAR. The arrows depict horizontal wind direction (orientation) and speed (length, scale to the lower right of the figure).

5.2.3 Errors due to changing wind directions over the rotor plane

Also large turnings of the wind speed with height over the rotor plane are frequently connected to the occurrence of low-level jets.

Again, profile measurements could lead to two further site characteristics: a mean vertical turning of the wind direction over the rotor plane (which could be calculated from Ekman-layer theory) and an extreme turning which can occur with a certain probability. Figure 29 shows an example from June 23, 1999 over a foreseen wind power site in Northern Germany. The measurement is a 10 minutes average, the situation lasted for several hours. Here turnings of up to 80 degrees were observed.

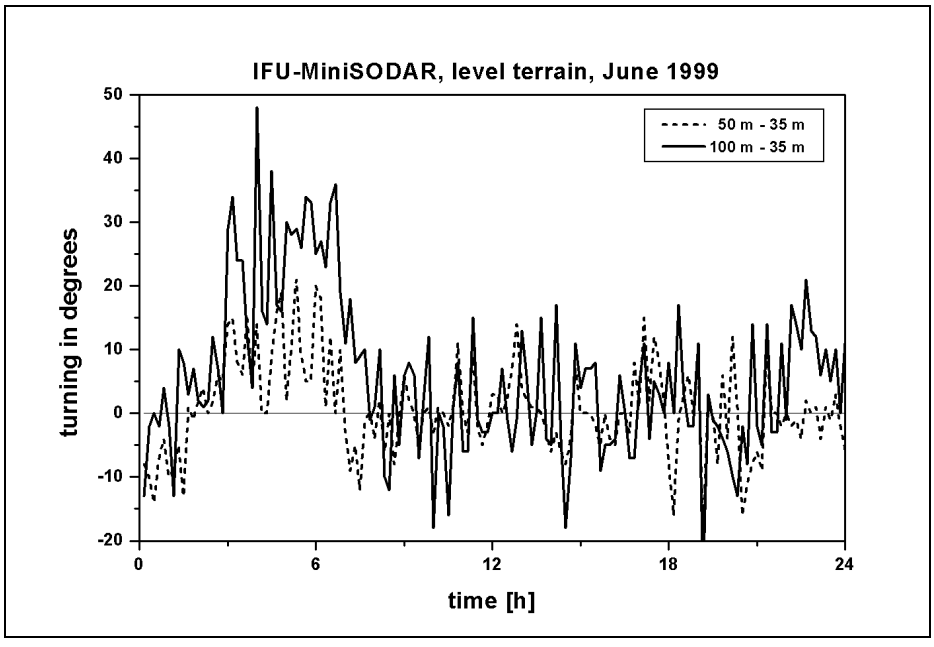

Figure 30 Monthly mean of wind turning with height over flat terrain in Northern germany in June 1999. Full curve: turning between 35 and 100 m, dashed curve: turning between 35 and 50 m above ground.

Such turnings are not seldom. Figure 30 shows the monthly mean of the turning of the wind with the vertical for June 1999 at a foreseen wind power site in Northern Germany. In early morning hours a mean turning of the wind direction between 35 and 100 m above ground of about 30 degrees can be observed for several hours. On the other hand, large turnings of wind direction with height are often coupled to low or moderate wind speeds, not to large wind speeds. This is depicted by Figure 31. For wind speeds of more than 8 m/s in 100 m above ground no turnings of more than 30 degrees between 60 and 160 m were observed.

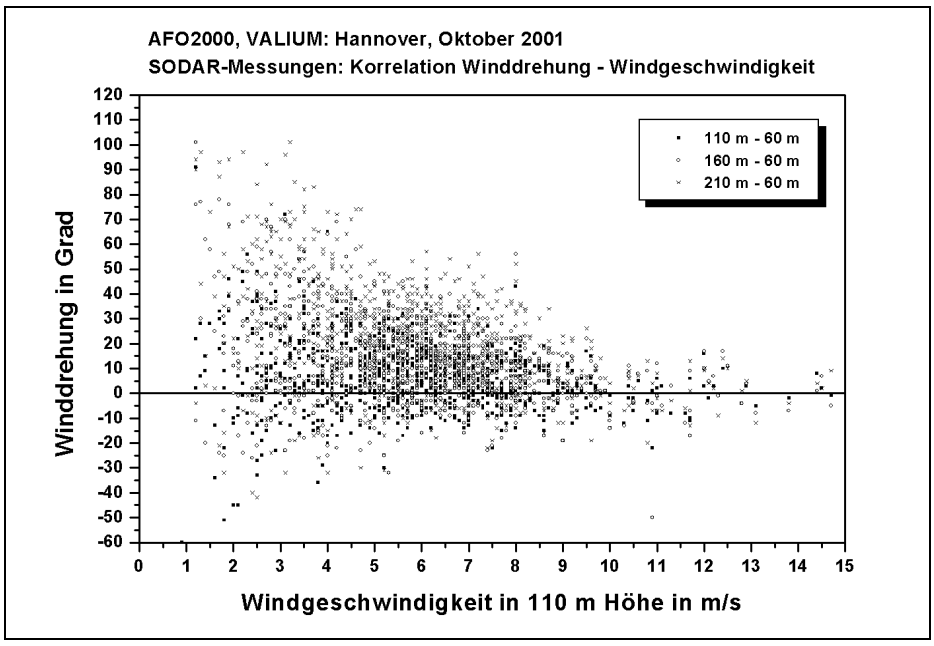

Figure 31 Correlation between mean wind speed in 100 m above ground and the turning of the wind between 80 and 110 m (full squares), 160 m (open circles), and 210 m (crosses).

The extreme case of June 23, 1999 has been taken as a basis for the evaluation plotted in Figure 32. Again wind turbines with relatively low hub heights are those that are affected most by possible wind turnings. But also turbines with very large rotor diameters have to take into account these effects in all possible hub heights.

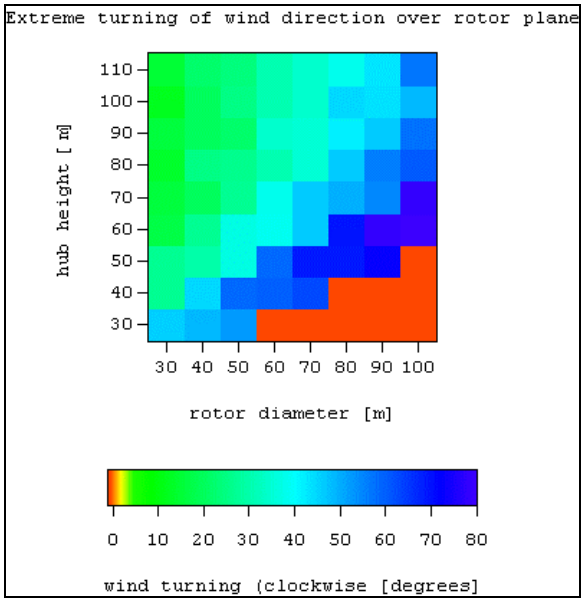

Figure 32 Extreme vertical gradient of wind direction as a function of hub height and rotor diameter in degrees derived from measurements by SODAR on June 23, 1999 over a foreseen wind power site in Northern Germany. Red area in the lower right corner: no data.

The wind turnings with height discussed so far have been connected to LLJs over flat terrain. In complex terrain wind turnings are probably as important as in the case discussed before. Mechanical and thermal effects of the orography can lead to large deviations in the lower layers from the geostrophic (or gradient wind) direction aloft. Mechanical effects can be the channelling of flow in valleys, the deviation of wind when blowing around a mountain, and recirculation features. Thermal effects can be upslope and downslope winds especially.

5.3 Vertical profiles of turbulence over the rotor plane

With respect to loads on blades and axes of wind turbines also the size and frequency of turbulence elements is important. These quantities can in principle be determined with profiling instruments. But the temporal resolution of a SODAR (one shot in the vertical direction every 10 to 30 seconds) is probably not sufficient to derive these quantities.

6. Cup anemometer measurements versus SODAR measurements

In the following a theoretical approach is given on the differences expected when the wind is measured using a cup and a SODAR anemometer. A quantification of these differences is attempted in order to explain why the cup and the SODAR anemometers measure different values of the wind speed. Four different factors, which affect the difference between cup and SODAR anemometers, have already been presented in Chapter 4.2. Here one of these four errors that is probably the largest one, the DP-error (Chapter 4.2.5), will be examined theoretically in more detail.

The SODAR wind speed measurements are usually made by taking the length of the average wind speed, here called vector averaging i.e. :

$$\vec{U}_i = \begin{pmatrix} x_i \\ y_i \\ z_i \end{pmatrix}$$

$$\left|\left\langle \vec{U} \right\rangle\right| = \sqrt{\left\langle x_i \right\rangle^2 + \left\langle y_i \right\rangle^2 + \left\langle z_i \right\rangle^2} \qquad \text{(Eq. 47)}$$

whereas the cup anemometer is measuring the instantaneous length of the instantaneous wind speed vector, here called speed averaging, defined as :

$$\left\langle \left|\vec{U}_i\right| \right\rangle = \sqrt{\left\langle x_i^2 \right\rangle + \left\langle y_i^2 \right\rangle + \left\langle z_i^2 \right\rangle} \qquad \text{(Eq.48)}$$

To describe the differences in the above equations we follow the idea of Kristensen (1999). Kristensen derived a formula for the difference between a vector speed and a cup speed. This is described in detail in the following. Instead of a Cartesian coordinate system we introduce a coordinate system where the instantaneous wind vector is aligned with respect to the mean wind direction, and is given by:

$$\vec{U}_i = \begin{Bmatrix} U \\ 0 \\ 0 \end{Bmatrix} + \begin{Bmatrix} u \\ v \\ w \end{Bmatrix} \qquad \text{(Eq. 49)}$$

Here U is the length of the mean wind speed vector and (u,v,w) are the turbulent perturbations.

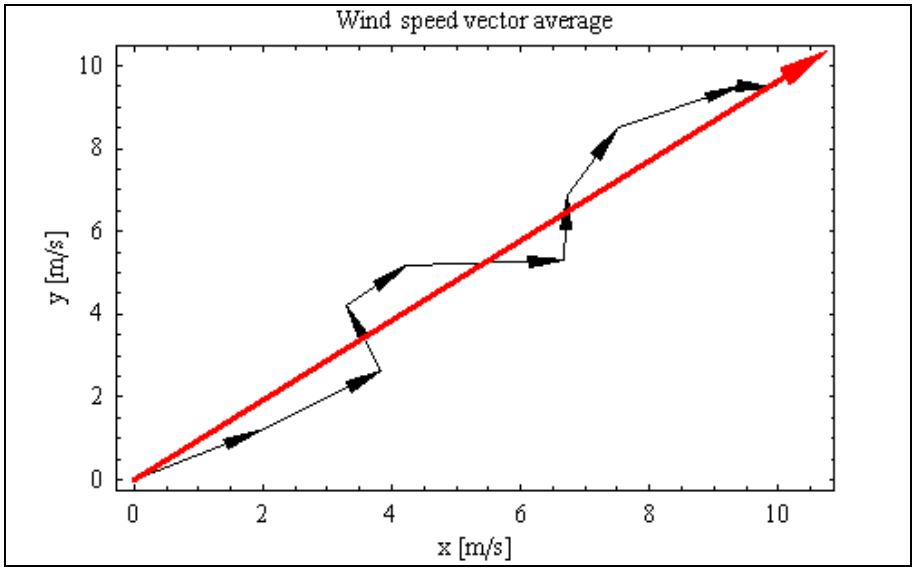

Figure 33 The average wind vector consists of contributions from the sum of the small wind vectors and the cup anemometer measures the sum of the lengths of the individual wind vectors, which is overestimated, compared to the total vector average.

The measured mean wind speed by a cup anemometer is now the horizontal projection of the total length of air which has passed through the instrument during the averaging time (which does not included directional changes). The measured average $\langle U_h \rangle$ is then (Kristensen 1999):

$$\langle U_h \rangle = \left\langle \sqrt{(U+u)^2 + v^2} \right\rangle$$

$$\langle U_h \rangle = U \left\langle \sqrt{1 + \frac{u^2}{U^2} + 2\frac{u}{U} + \frac{v^2}{U^2}} \right\rangle$$

$$\langle U_h \rangle \approx U \left\langle 1 + \frac{1}{2}\left(\frac{u^2}{U^2} + 2\frac{u}{U} + \frac{v^2}{U^2} \right) - \frac{1}{8}\left(\frac{u^2}{U^2} + 2\frac{u}{U} + \frac{v^2}{U^2} \right)^2 + O\left[\left(\frac{u^2}{U^2} + 2\frac{u}{U} + \frac{v^2}{U^2} \right) \right]^3 \right\rangle \quad \text{(Eq. 50)}$$

$$\langle U_h \rangle \approx U + \frac{\langle v^2 \rangle}{2U}$$

Here U is the average length of the wind speed vector and *u* and *v* are the fluctuations. All terms of order higher than 2 as well as the vertical velocity terms have here been neglected.

The horizontal fluctuations $\langle v^2 \rangle$ in the neutral surface layer can be parameterised by (Panofsky et al 1977):

$$\frac{\langle v^2 \rangle}{u_*^2} \approx 2.3^2 \quad \text{(Eq. 51)}$$

where u_* is the friction velocity.

By introducing the neutral logarithmic wind profile :

$$U(z) = \frac{u_*}{\kappa} Ln(z/z_0) \quad \text{(Eq. 52)}$$

we can now express the difference between the scalar averaging $\langle U_h \rangle$ and vector average length U solely by the measurement height and roughness z_0 by combining Eq. 49 to Eq. 51 which gives:

$$\langle U_h \rangle = U\left(1+\frac{2.5^2}{2}\frac{\kappa^2}{Ln(z/z_0)^2}\right) \qquad \text{(Eq. 53)}$$

In Figure 34 the effects of different roughness and thereby also different turbulence intensities are shown for six heights ranging from 50 to 100 m.

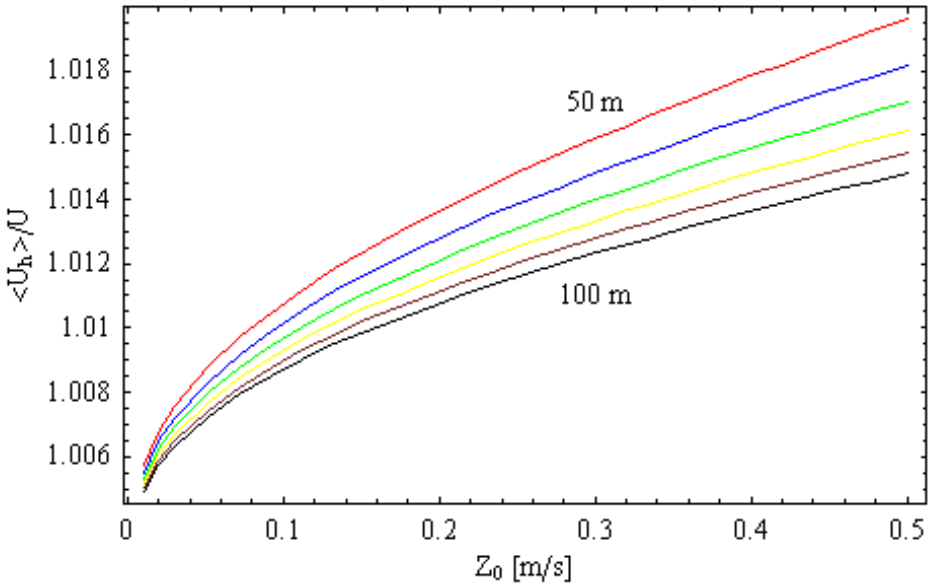

Figure 34. The ratio of the measured wind speed with a cup anemometer and the vector averaged wind speed as a function of the roughness. Here a higher roughness also indicates more turbulence. The red curve shows the ratio at 50 m and the black curve is the values at 100m, the curves in between are heights with an interval of 10 m.

In the free convective situations the velocity fluctuations are increased which will be shown in the following. The wind speed profile under convective situations are given by (Panofsky et al. 1977):

$$U(z) = \frac{u_*}{\kappa}\left[Ln(z/z_0) - \Psi(z/L)\right]$$
$$\Psi(z/L) = 2Ln\left(\frac{1+x}{2}\right) + Ln\left(\frac{1+x^2}{2}\right) - 2Arc\tan(x) + \frac{\pi}{2} \qquad \text{(Eq. 54)}$$
$$x = (1-15\,z/L)^{1/4}$$

where L is the Monin-Obukov length defined as :

$$L = \frac{u_*^2}{\kappa\beta T_*}$$
$$T_* = \frac{\overline{w'\theta'}}{u_*}, \quad \beta = g/T_o \qquad \text{(Eq. 55)}$$

here $\rho c_p \overline{w'\theta'}$ is the heat flux and β is the buoyancy parameter. The convective situations are here characterised with values of $z/L < 0$.

The normalized turbulence fluctuations are given by (Panosky et al. 1977):

$$\frac{\sigma_v}{u_*} = \left(12 - 0.5 h/L\right)^{(1/3)} \qquad \text{(Eq. 56)}$$

h is the boundary layer height which under convective situations often is in the order of 1 km.

In Figure 35 the relation $<U_h>/U$ is shown as function of the $-L$ and z_0 with an inversion height of 1000m and a measurement height of 100m. The figure shows that for free convection over rough surfaces the error becomes in the order of 2 %.

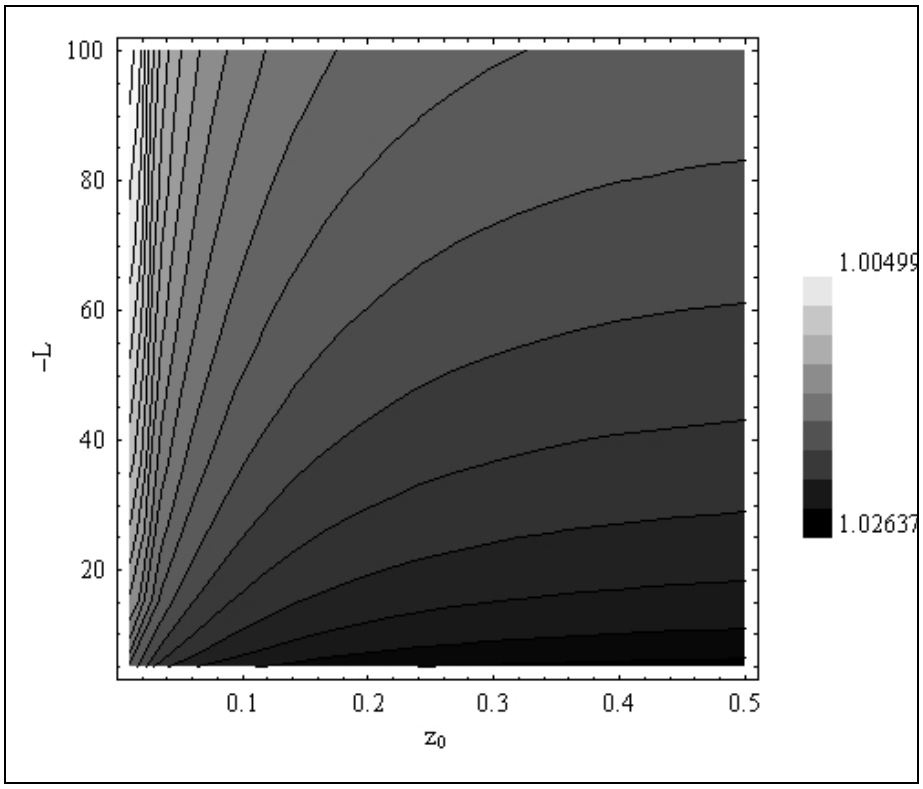

Figure 35 A contour plot of $<U_h>/U$ *as function of respective the roughness and L . Largest differences are obtained for very convective situations with L near zero and large roughness resulting in the largest wind speed fluctuations.*

The difference between the measured cup speed and vector speed also depends of the height above the ground as shown in Figure 36. Here the difference between the two ways to obtain the wind speed decrease with height for given a specified atmospheric stability is shown.

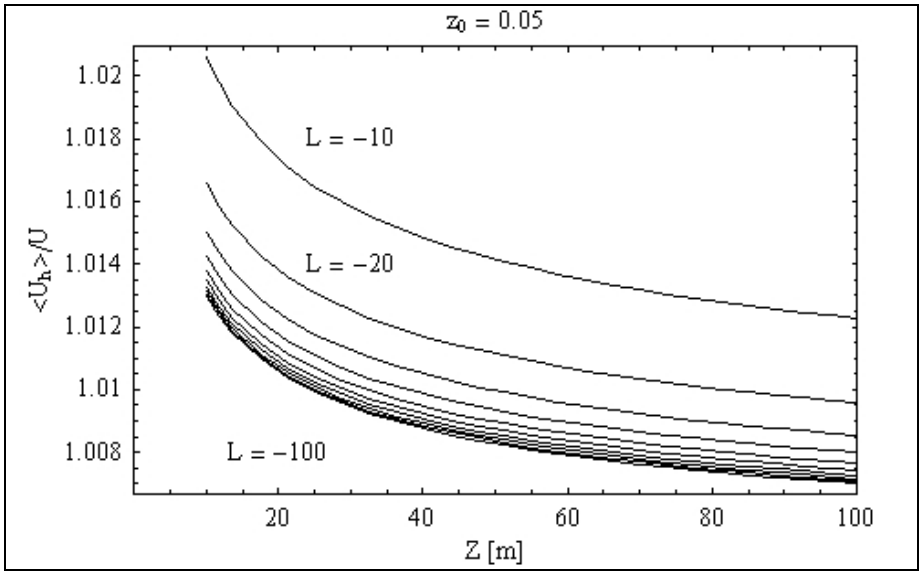

Figure 36 The ratio of $<U_h>/U$ *as function of the height for a give roughness. The different curves represent the different atmospheric stabilities.*

6.1 Conclusions from the comparison of cup and SODAR measurements

The overall conclusions of the above analysis, which is in good agreement with the experimental findings on the DP-error in Chapter 4.2.4, is that in the comparison between cup anemometers and SODARs, there will always be a bias in the regression i.e.:

$$U_{Sodar} = \alpha U_{cup} \qquad \text{(Eq. 57)}$$

where $\alpha < 1$ and with values in the order of 0.98 to 0.995. In previous comparisons (Jørgensen and Antoniou (2002)) there is some evidence of this, when a regression line with no offset value is chosen. Values higher than one can of course appear due to the statistical scatter from the data. Together with the systematic u-error (Chapter 4.2.2) that is in the order of 1%, one can expect an α with values in the order of 0.97 to 0.995.

Another cause for the deviations can be attributed to the fact that there is a possible under speeding from cup anemometers as opposed to what we have described above. This is caused due to the fact the anemometers have a cosine response as regard to the vertical deviations. Consider Figure 33 and imagine that the perturbations now are in the vertical direction and the mean vector represents the horizontal plane. The length of the instantaneous vectors is then underestimated due to the cosine response of the cup, hence the total length of the average vector is therefore underestimated. However, Kristensen (2002) showed that this has a minor effect compared to the horizontal fluctuations by the *v* component and therefore negligible for all practical purposes.

7. Comparison of wind power estimates from point and profile measurements

The practicability of the profile descriptions (44) and (46) is demonstrated in Figure 37 by evaluating vertical profiles of the available wind energy.

In level terrain the curve using A- and k-profiles from (44) and (46) fits well to the observed curve at heights above 50 m above ground. The underestimation below 50 m comes from the underestimation of A(z) by (44) in this height range (see Figure 18). On the hill top the curve using A- and k-profiles from (44) and (46) follows the measured curve well between 50 m and 100 m above. The deviation above 100 m comes from the underestimation of k(z) by (46) in this height range (see Figure 19), the

deviation below 50 m stems from an underestimation of A(z) by (44) in that height range (see Figure 18). For comparison also those wind energy profiles have been plotted which would result from an application of the power law (41) and the k-profiles (45) proposed by Justsus et al. (1978) and Allnoch (1992). The latter profiles overestimate the available wind energy in level terrain, but underestimate the wind energy over hill tops. The energy profiles from WAsP do not differ very much between the two sites and are close to the estimations for the site in level terrain.

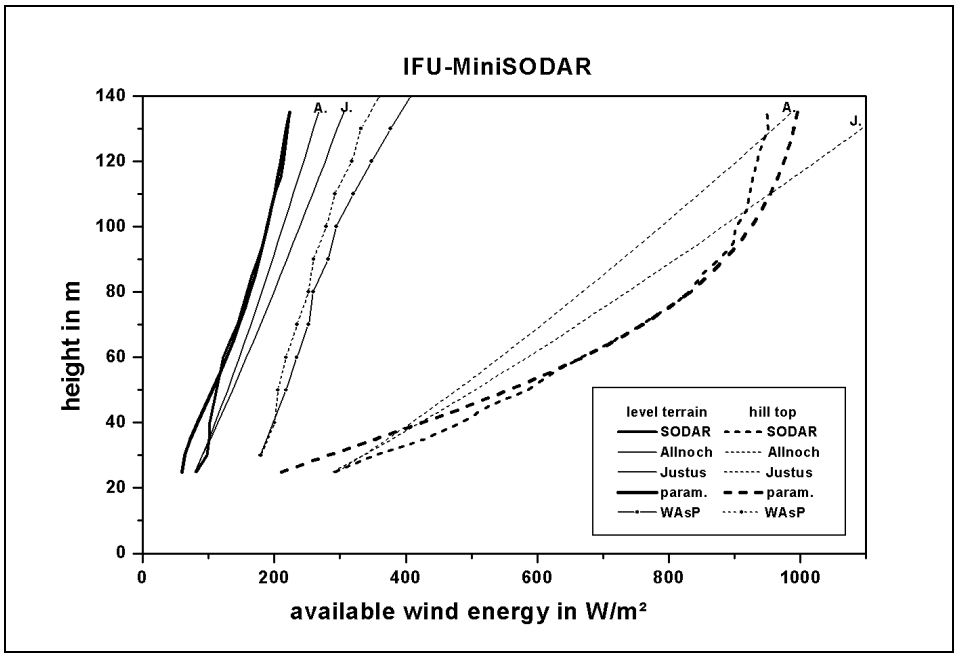

Figure 37 Parameterised vertical profiles of the available wind energy.

8. The influence of wind shear and turbulence on the turbine performance

Both the shape and the turbulence content of the wind regime influences the performance of the wind turbine and because of this their measurement is of importance for wind energy purposes. This is the reason why the measurement of the wind speed at the center of the turbine rotor is not adequate, especially since the new rotors and the turbine's hub height have reached dimensions of the order of hundred meters. At these sizes many meteorological parameters, such as the stratification of the atmosphere, influence the shape of the wind profile and may influence the production and the electrical efficiency of the turbine. Therefore the measurement of the wind speed should take place at more heights and the SODAR, in such situations, is in principle more appropriate for the measurement of the wind speed. Nevertheless the measurement of turbulence is also important and the SODAR is not, until further work is done on this subject, suitable for this measurement.

In the following the results of such an investigation are presented. The wind profile in front of a turbine has been measured at more heights using cup anemometers. The accurate measurement of the wind shear using cup anemometers is not without problems, as the boom-mounted cup anemometers need to be kept away from the influence of the met mast and this can only be achieved by both using adequate long booms and by excluding a part of the measurement sector. From these results the mean wind profile during the tests has been derived using an exponential fit. The mean wind speed results over the rotor are compared to the results read by the cup anemometer at hub height.

The atmospheric stability has also been measured by using the temperature difference at two heights. The turbulence intensity is a function of the atmospheric stability as a stable/unstable atmosphere is as a rule well correlated to low/high turbulence intensities.

The turbine is a 3MW turbine with a hub height of 57m and a diameter of 80m. The influence of the wind regime on the turbine performance has been investigated with the help of the experimental results and calculations. The calculations have taken place by using the aeroelastic code FLEX5.

The aim has been to investigate the influence of the wind shear and turbulence on the electrical power and the electrical power coefficient, and explain the reasons for the rather low Cp values observed during the tests. In the wind energy industry, the behavior of the turbine is important as it is connected to production warranties. Failure to comply with these may have serious consequences for the manufacturer or the wind farm developer.

8.1 The wind shear during the measurement period

The differential temperature at the site was measured using a differential temperature sensor at 54m and 12m heights, Figure 38. The differential temperature is an approximate measure of the atmospheric stability. As a rule the temperature falls with app. 1° per 100m height and following the results of the figure, the temperature difference attained mostly positive values during the measurement period. Hence the results show that the atmosphere has been predominately stable during the period of the tests, at the heights investigated.

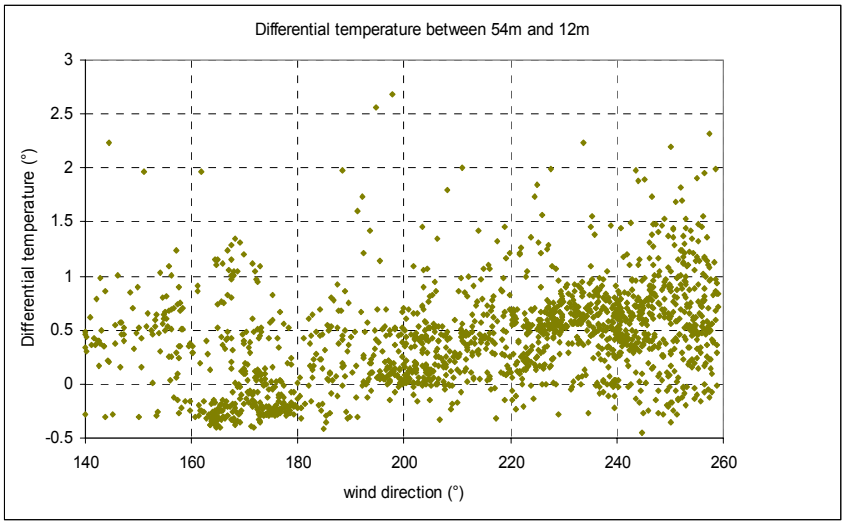

Figure 38 The differential temperature between 54m and 12m height

As a rule, in a stable atmosphere, turbulence production is suppressed and the wind profile is characterised by high values of the shear exponent. The low turbulence intensity during the measurement period is shown in Figure 39.

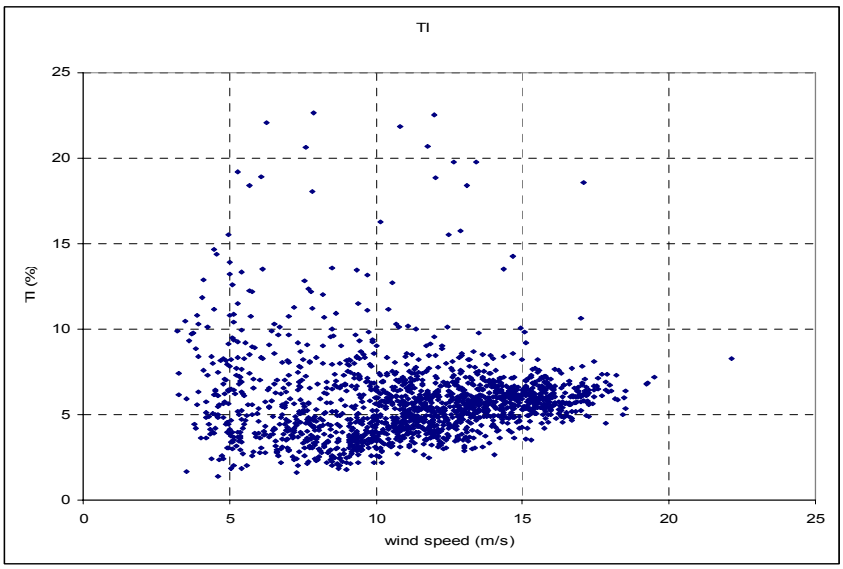

Figure 39 The turbulence intensity during the measurement period

The large shear is illustrated by the following results. On the met mast, cup anemometers were mounted at 25m, 41m and 57m (hub height). The anemometers at 25 and 41m are mounted on booms while the anemometer at 57m is mounted at the top of the mast. In order to minimise the influence from the presence of the tower a narrow sector of ±30° around the mast-turbine direction was chosen. In these data an exponential profile has been fitted through the three heights, Figure 40, following the power low for wind profiles:

$$V(z)=Vhub*(z/zhub)^a$$

An exponent of 0.24 fits the data. In the same figure the wind profile for an exponent equal to 0.1, typical of profiles over water is shown.

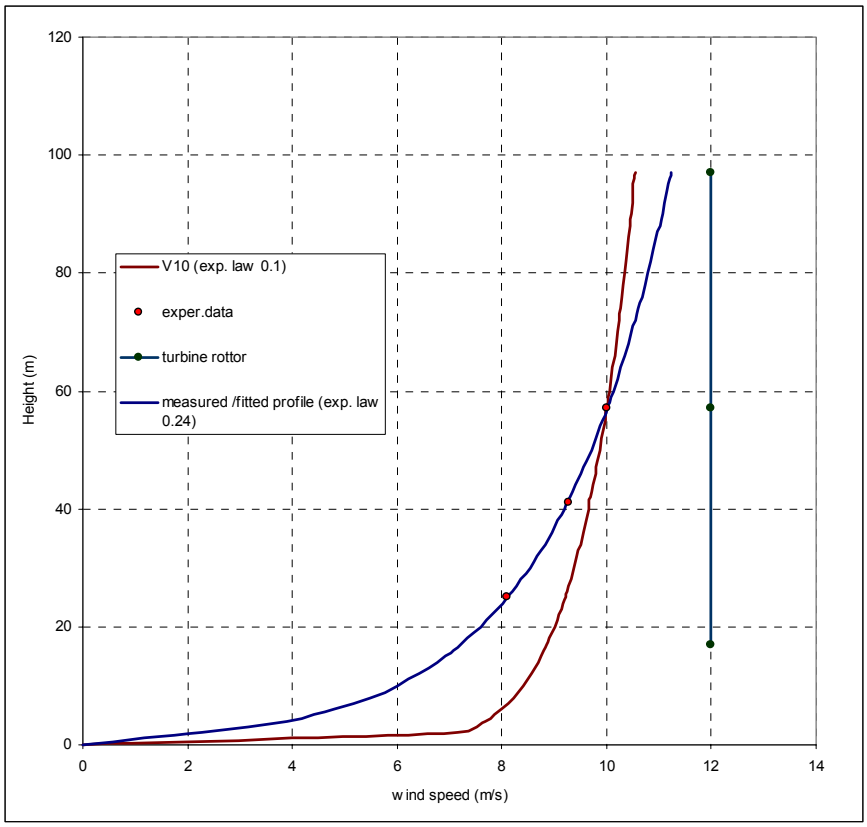

Figure 40 The wind profile over the turbine rotor for a hub height value equal to 10m/s.

The results are not valid for the whole measurement sector, as the readings of the anemometers at 25m and 41m, would be disturbed from the met tower presence. However as the surroundings are flat and the atmospheric conditions alike, similar profiles with high shear exponents should be expected also from other wind directions.

As a result of the large shear, the mean wind speed value over the turbine rotor is lower for a shear exponent of 0.24, as compared to the mean wind speed for a profile with an exponent of 0.1 and for the same wind speed at hub height. The difference is of the order of 1%. The influence of this on the power production of the turbine will later be quantified with the help of the FLEX5 code.

8.2 The influence of the atmospheric turbulence on the power curve and the electrical efficiency

The influence of the turbulence on the power curve and the electrical efficiency of the turbine is investigated by filtering the experimental data successively for turbulence intensities less than 3.5%, 4.0%, 4.5% and 5%. The results are shown in the following Figure 41 and Figure 42 and the corresponding bin values in the following Table 2. The original data set is also included for comparison purposes. Filtering the lower turbulence intensities results effectively in an increase of the turbulence intensity in the corresponding bin. The increase in turbulence is seen to result in an increase in the power and the corresponding Cp values.

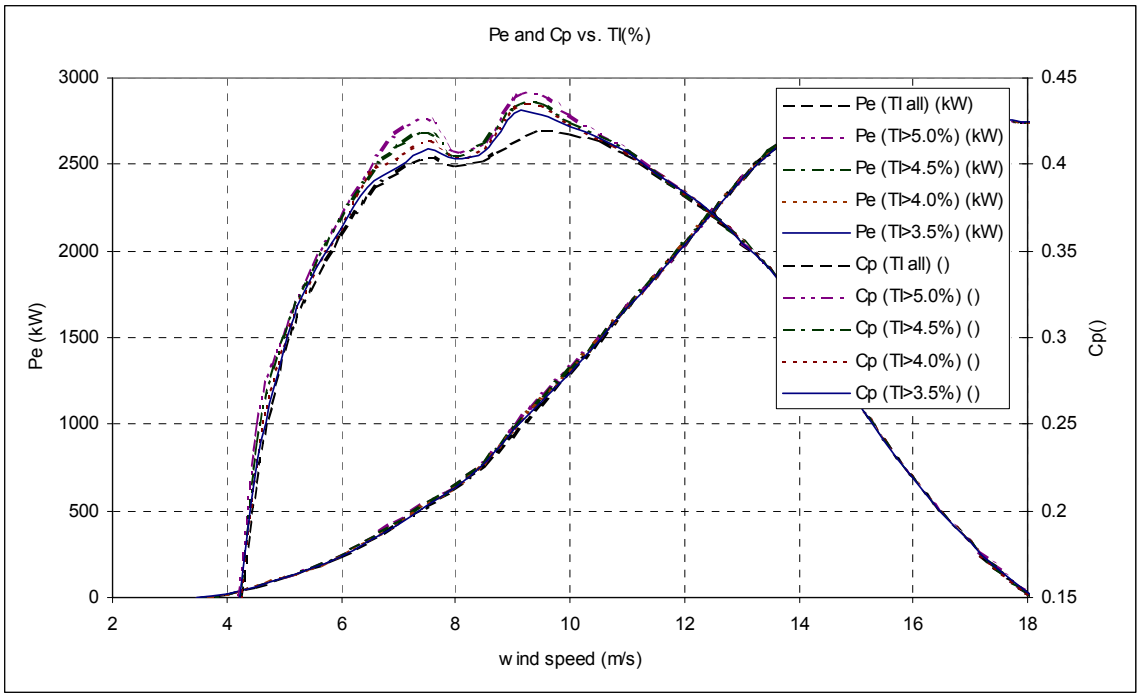

Figure 41 The electrical power and the electrical efficiency of the turbine when filtering the data for the lowest turbulence intensities.

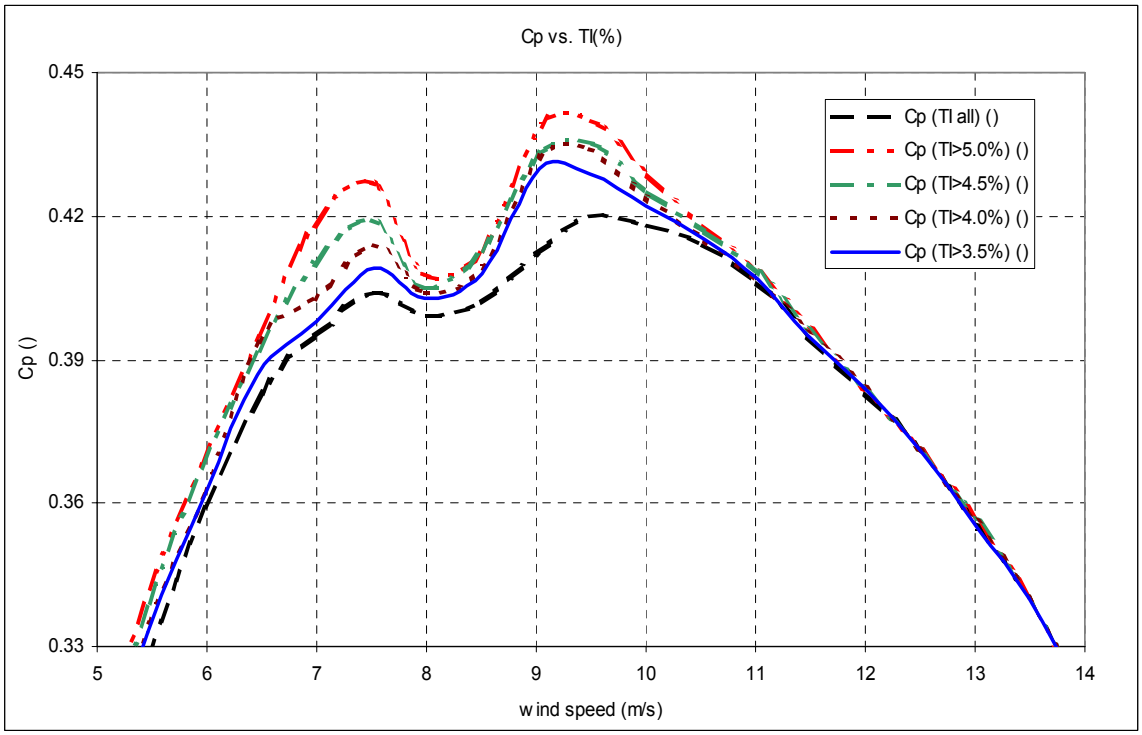

Figure 42 The electrical efficiency of the turbine when the lower turbulence data are filtered away (detail)

Table 2 The bin values of the filtered and the original data

TI > 3.5%					TI > 4.0%					TI > 4.5%					TI > 5.0%					TI all				
WspHub_cor	Turb	Pe (TI>3.5%)	Cp (TI>3.5%)	No	WspHub_cor	Turb	Pe (TI>4.0%)	Cp (TI>4.0%)	No	WspHub_cor	Turb	Pe (TI>4.5%)	Cp (TI>4.5%)	No	WspHub_cor	Turb	Pe (TI>5.0%)	Cp (TI>5.0%)	No	WspHub_cor	Turb	Pe (TI>0.0%)	Cp (TI>0.0%)	No
(m/s)	(%)	(kW)	()	()	(m/s)	(%)	(kW)	()	()	(m/s)	(%)	(kW)	()	()	(m/s)	(%)	(kW)	()	()	(m/s)	(%)	(kW)	()	()
3.472	8.41	1.246	0.01	7	3.472	8.406	1.246	0.01	7	3.472	8.41	1.246	0.01	7	3.472	8.41	1.246	0.01	7	3.482	7.56	-1.184	-0.009	8
4.008	7.29	18.084	0.091	17	3.991	7.775	14.859	0.076	15	4.018	8.31	16.775	0.084	13	4.001	8.60	18.341	0.093	12	4.008	7.29	18.084	0.091	17
4.492	6.66	60.572	0.217	26	4.5	7.014	64.163	0.229	23	4.513	7.43	67.827	0.24	20	4.517	7.88	70.851	0.25	17	4.5	6.18	60.518	0.216	29
5.008	7.14	114.09	0.295	43	4.991	7.799	113.046	0.295	36	4.993	8.12	114.832	0.3	33	4.999	8.46	116.857	0.304	30	5.011	6.32	113.351	0.293	53
5.461	7.50	167.067	0.333	36	5.475	7.96	169.339	0.335	32	5.473	8.20	171.318	0.339	30	5.474	8.72	172.685	0.342	26	5.46	6.82	164.014	0.327	42
5.979	7.08	237.805	0.362	24	5.979	7.947	238.483	0.362	19	5.949	8.39	238.209	0.367	17	5.948	8.63	238.158	0.368	16	5.985	6.34	237.253	0.359	29
6.462	6.72	321.161	0.387	27	6.483	7.378	330.08	0.394	22	6.471	8.10	327.023	0.392	18	6.471	8.29	329.826	0.395	17	6.5	6.03	323.822	0.383	33
6.999	5.52	419.87	0.398	41	6.981	6.029	422.294	0.403	32	6.962	6.62	426.396	0.41	24	6.97	7.12	435.631	0.418	19	6.991	5.13	415.343	0.395	48
7.523	6.50	535.816	0.409	42	7.516	6.857	540.851	0.414	37	7.512	7.07	546.666	0.419	34	7.514	7.69	557.159	0.427	27	7.519	5.65	528.227	0.404	54
7.981	6.35	630.918	0.403	36	7.983	6.888	632.154	0.404	30	7.97	7.85	630.492	0.405	22	7.971	9.30	636.473	0.408	15	7.996	5.34	627.907	0.399	51
8.512	6.76	775.571	0.408	30	8.5	7.217	773.78	0.409	26	8.5	7.59	781.248	0.413	23	8.51	7.73	784.183	0.413	22	8.506	5.32	762.536	0.402	47
9.033	6.03	975.51	0.43	33	9.025	6.254	978.131	0.432	30	9.03	6.55	981.116	0.433	26	9.042	7.07	999.38	0.439	20	9.006	4.63	927.096	0.412	56
9.498	6.25	1131.96	0.429	53	9.499	6.898	1143.82	0.434	42	9.517	7.18	1155.32	0.435	38	9.513	7.84	1164.946	0.44	30	9.497	5.24	1107.105	0.42	78
10	5.60	1298.29	0.422	70	9.998	6.062	1304.56	0.424	56	10.014	6.51	1313.8	0.425	45	10.009	7.06	1324.397	0.429	34	10.013	5.14	1291.586	0.418	85
10.535	5.64	1493.31	0.415	63	10.544	5.897	1498.86	0.415	55	10.534	6.40	1499.94	0.417	42	10.526	6.76	1499.557	0.418	35	10.524	5.32	1484.142	0.414	72
11.017	5.68	1673.36	0.407	92	11.016	5.911	1675.08	0.407	82	11.024	6.32	1680.9	0.408	66	11.036	6.75	1688.724	0.408	52	11.015	5.57	1671.983	0.406	96
11.482	5.49	1842	0.395	93	11.484	5.603	1844.75	0.396	87	11.48	5.76	1845.78	0.396	78	11.501	6.36	1852.764	0.396	49	11.48	5.34	1839.097	0.395	99
11.997	5.77	2039.26	0.384	92	12.002	6.196	2041.53	0.384	76	11.99	6.69	2038.43	0.384	61	11.972	7.26	2030.843	0.384	47	12	5.59	2037.164	0.383	99
12.507	6.07	2235.22	0.371	68	12.499	6.345	2231.96	0.371	61	12.495	6.66	2230.48	0.371	53	12.501	7.05	2230.667	0.371	44	12.502	5.84	2229.503	0.371	74
13.019	5.94	2414.89	0.355	82	13.019	6.114	2419.43	0.356	76	13.028	6.25	2422.62	0.356	71	13.044	6.53	2428.39	0.355	60	13.015	5.75	2411.24	0.355	88
13.487	6.05	2565.01	0.34	84	13.487	6.1	2565.64	0.34	82	13.486	6.17	2568.7	0.34	79	13.493	6.35	2567.558	0.34	70	13.485	5.98	2564.063	0.34	86
13.986	5.89	2683.55	0.319	63	13.984	5.924	2683.28	0.319	62	13.98	6.07	2679.64	0.319	57	13.973	6.29	2674.124	0.318	48	13.981	5.80	2680.426	0.319	65
14.483	5.99	2735.53	0.293	70	14.481	6.057	2735.04	0.293	68	14.48	6.11	2734.82	0.293	66	14.483	6.29	2732.63	0.292	58	14.483	5.99	2735.531	0.293	70
14.967	5.96	2747.23	0.266	64	14.966	6.002	2747.14	0.266	63	14.967	6.09	2746.78	0.266	60	14.969	6.30	2745.733	0.266	52	14.97	5.93	2747.336	0.266	65
15.486	6.05	2751.96	0.241	66	15.486	6.046	2751.96	0.241	66	15.481	6.10	2752.03	0.241	64	15.484	6.14	2752.008	0.241	62	15.486	6.05	2751.958	0.241	66
15.96	6.08	2751.48	0.22	68	15.96	6.079	2751.48	0.22	68	15.96	6.08	2751.48	0.22	68	15.966	6.14	2751.602	0.22	65	15.96	6.08	2751.477	0.22	68
16.493	5.64	2750.08	0.199	33	16.493	5.639	2750.08	0.199	33	16.493	5.64	2750.08	0.199	33	16.491	5.91	2751.18	0.199	25	16.493	5.64	2750.076	0.199	33
16.983	6.58	2751.57	0.182	37	16.983	6.581	2751.57	0.182	37	16.983	6.58	2751.57	0.182	37	16.98	6.73	2751.503	0.183	34	16.983	6.58	2751.567	0.182	37
17.445	6.22	2752.02	0.168	15	17.445	6.221	2752.02	0.168	15	17.445	6.22	2752.02	0.168	15	17.424	6.34	2751.886	0.169	14	17.445	6.22	2752.016	0.168	15
17.992	6.74	2751.07	0.153	10	17.992	6.735	2751.07	0.153	10	17.992	6.74	2751.07	0.153	10	17.992	6.74	2751.07	0.153	10	17.992	6.74	2751.07	0.153	10
18.422	5.75	2753.03	0.143	6	18.422	5.747	2753.03	0.143	6	18.422	5.75	2753.03	0.143	6	18.443	5.90	2752.563	0.143	5	18.422	5.75	2753.031	0.143	6
19.05	6.81	2751.94	0.129	2	19.05	6.814	2751.94	0.129	2	19.05	6.81	2751.94	0.129	2	19.05	6.81	2751.938	0.129	2	19.05	6.81	2751.938	0.129	2
19.326	7.16	2751.6	0.124	1	19.326	7.162	2751.6	0.124	1	19.326	7.16	2751.6	0.124	1	19.326	7.16	2751.601	0.124	1	19.326	7.16	2751.601	0.124	1
21.927	8.30	2752	0.085	1	21.927	8.299	2752	0.085	1	21.927	8.30	2752	0.085	1	21.927	8.30	2751.997	0.085	1	21.927	8.30	2751.997	0.085	1
			Total	1495				Total	1358				Total	1220				Total	1026				Total	1683

The above analysis shows that there exists a direct connection between the turbulence intensity and the electrical power and efficiency of the turbine. At the same time the filtering influences the mean value of the shear exponent but due to lack of data this influence cannot be quantified.

8.3 Numerical simulations using the FLEX5 code.

The operation of the turbine has been simulated using the FLEX5 code. The power curve of the turbine has been calculated for a combination of turbulence intensities ranging from TI=0.0% to TI=10% and wind profiles with exponents ranging from a=0.1 to a=0.25. The results are presented below for three wind speeds, below maximum Cp (V=7m/s), at maximum Cp (V=9m/s) and above maximum Cp (V=11m/s).

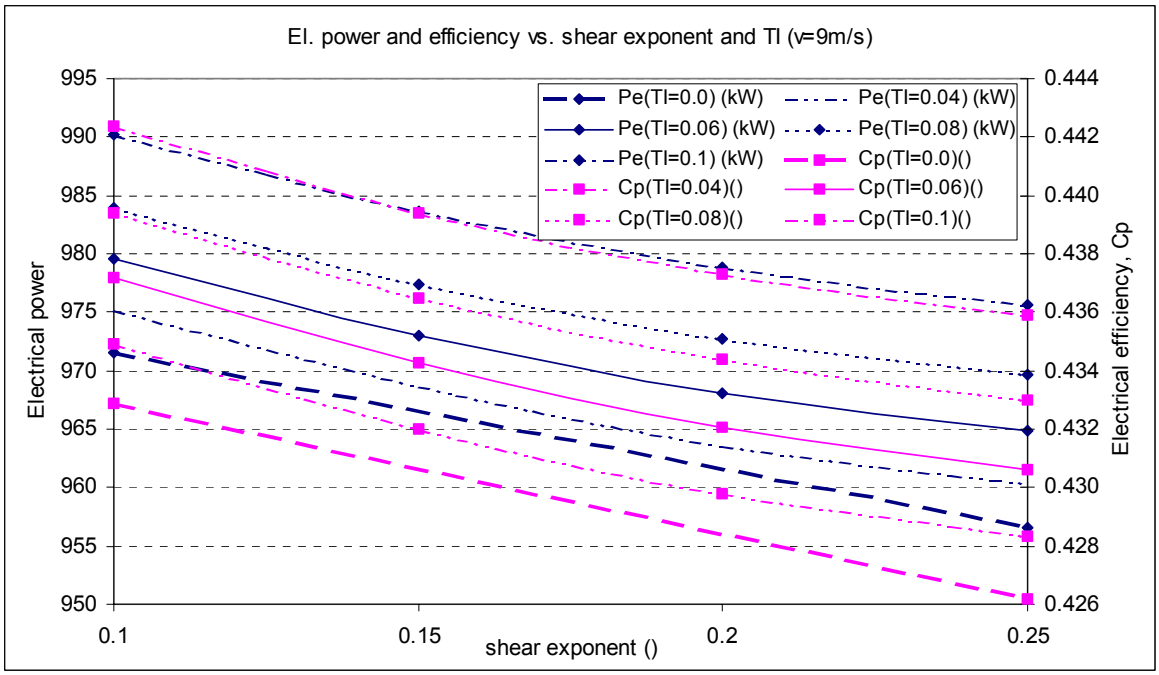

Figure 43 FLEX5 simulations for V=9m/s

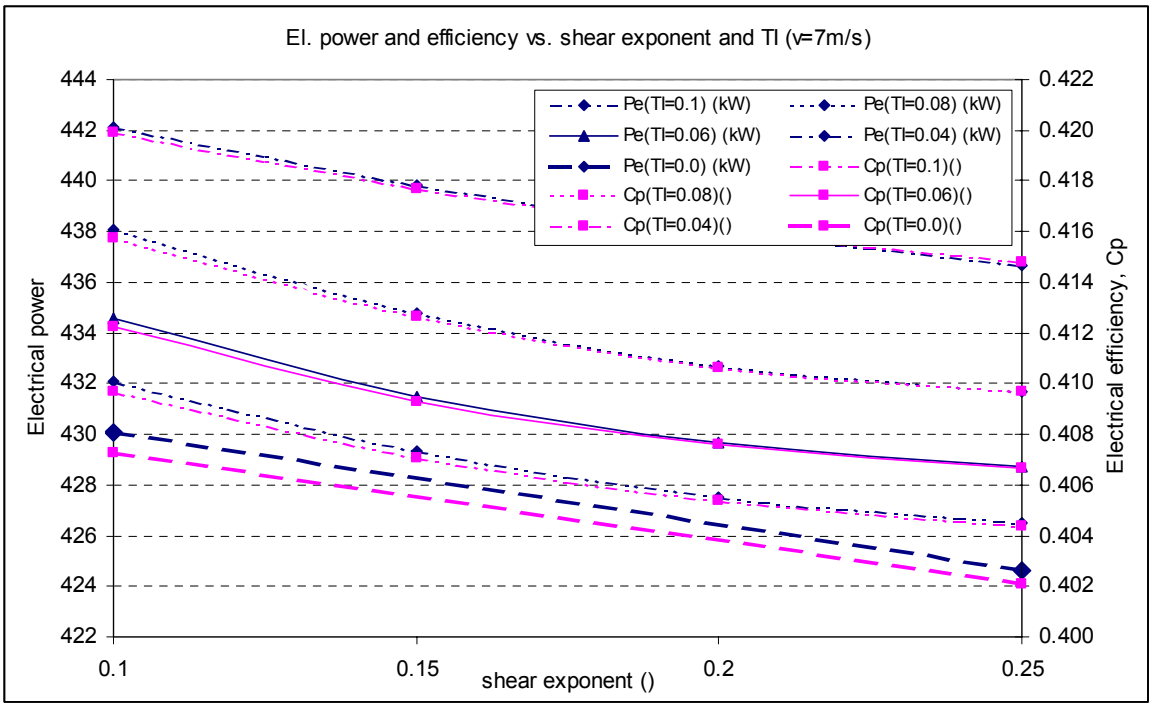

Figure 44 FLEX5 simulations for V=7m/s

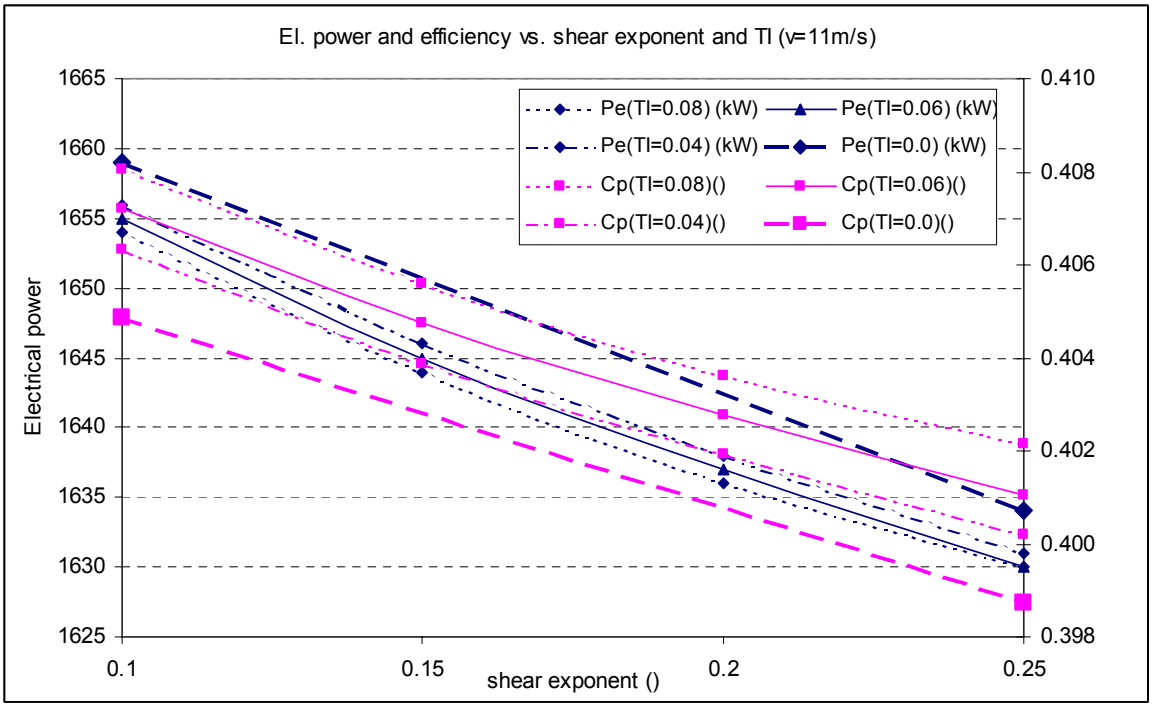

Figure 45 FLEX5 simulations for V=11m/s

The FLEX5 simulations show that for wind speeds around max Cp, the increase in wind shear results in a reduction of both the electrical power and the electrical efficiency. For a given wind shear an increase in the turbulence intensity, increases both the electrical power and efficiency.

A comparison of Figure 43 and Table 2 shows a close agreement between the experimental data and the FLEX5 simulation results.

8.4 Conclusions on the influence of wind shear and turbulence on the wind turbine behaviour

The influence of the wind profile shape and the turbulence intensity on the power output and hence the electrical efficiency of the wind turbine has been investigated using the experimental data and simulation results using the FLEX5 code. The results show a clear tendency for higher Cp values due to higher turbulence intensities and lower wind shear exponents. Thus the need for the registration of the wind profiles within the rotor disk is evident. Both the wind shear and the turbulence intensity play an important role on the determination of the turbine behaviour.

9. Conclusions

A number of issues regarding SODARs and the measurement of the atmospheric wind speed with the use of either them or / and cup anemometers have been addressed in the present report. The measurement principle is different between SODARs and cup anemometers with the largest difference being that of a point and a volume measurement.

The SODAR presents a number of advantages in the measurement of the wind speed in connection with wind energy applications, relative to the use of a cup anemometer. These advantages are related to the ability of the SODAR to measure the wind speed profile simultaneously at more heights. As shown in the present report the measurement at the center of the rotor disk is not always representative of the wind speed over the whole rotor and the differences are increasing with the increase of the wind shear. Also the expenses associated to the purchase of a met mast increase considerably as the height of the mast increases.

Among the drawbacks of the measurements when using the SODAR are the limitations due to the background noise at high wind speeds or the neutral condition of the atmosphere. Finally the systematic bias in the measurements, between the cup and the SODAR anemometer results, which both the experimental analysis and the theoretical results point at, is important in the sense that it adds to the uncertainty of the measurement.

10. References

Albers, A., H. Klug and D. Westermann, 2001: Cup Anemometry in Wind Engineering, Struggle for Improvement. DEWI Magazin Nr. 18 (February 2001), 17-28.

Allnoch, N., 1992: Windkraftnutzung im nordwestdeutschen Binnenland: Ein System zur Standortbewertung für Windkraftanlagen. Geographische Kommission für Westfalen, Münster, ARDEY-Verlag (cited from Hänsch 1997).

Busch, N.E., 1965: A micrometeorological data-handling system and some preliminary results. Risø Report No. 99, 92 pp.

Busch, N.E. and L. Kristensen, 1976: Cup anemometer overspeeding. J. Appl. Meteorol., **15**, 1328-1332.

Businger, J.A., J.C. Wyngaard, Y. Izumi and E.F. Bradley, 1971: Flux profile relationships in the atmospheric surface layer. J. Atmos. Sci., **28**, 181-189.

Corsmeier, U., N. Kalthoff, O. Kolle, M. Kotzian and F. Fiedler, 1997: Ozone concentration jump in the stable nocturnal boundary layer during a LLJ-event. Atmosph. Environm., **31**, 1977-1989.

Crescenti, G.H., 1997: A look back on two decades of Doppler SODAR comparison studies. Bull. Amer. Meteorol. Soc., **78**, 651-673.

Davenport, A.G., 1965: The relationship of wind structure to wind loading. Nat. Phys. Lab. Symp. No. 16 "Wind effects on buildings and structures", 54-112. Her Majesty's Staionary Office, London.

Dyer, A.J., 1974: A review of flux-profile relations. Bound.-Lay. Meteorol., **1**, 363-372.

Emeis, S., 2001: Vertical variation of frequency distributions of wind speed in and above the surface layer observed by SODAR. Meteorol. Z., **10**, 141-149.

Hau, E., 2002: Windkraftanlagen - Grundlagen, Technik, Einsatz, Wirtschaftlichkeit. 3rd edition. Springer Berlin, Heidelberg, etc. 792 pp.

Jørgensen, H.E.; Antoniou, I., Inter comparison of two commercially available SODARS. Risø-R-1383(EN)(2002) 23 p. Risø-R rapport

Justus, C.G., W.R. Hargraves, A. Mikhail und D. Graber, 1978: Methods for estimating wind speed frequency distributions. J. Appl. Meteorol., **17**, 350-353 (cited from Hänsch 1997).

Kaimal, J. C., 1986: Flux and profile measurements from towers in the boundary layer. In: *Probing the Atmospheric Boundary Layer,* D. H. Lenschow, (Ed.), Amer. Meteor. Soc., 19–28.

Kirtzel, H.J., Peters, G., 1999 “Grundlagen der SODAR-Technik und Leistungsfähigkeit moderener SODAR-Geräte”, in “Berichte der Strahlenschutzkommission (SSK) des Bundesministeriums für Umwelt, Naturschutz und Reaktorsicherheit”, **22.**

Kottmeier, C., D. Lege and R. Roth, 1983: Ein Beitrag zur Klimatologie und Synoptik der Grenzschichtstrahlströme über der norddeutschen Tiefebene. A.. Meteorol. (N.F.), **23**, 18-19.

Kristensen, L., 1993: The cup anemometer and other exciting instruments. Doctor thesis at the Technical University of Denmark in Lyngby. Risø National Laboratory, Roskilde, Denmeark. Risø-R-615 (EN), 83 pp.

Kristensen, L., The perennial cup anemometer. Wind Energy (1999) **2** , 59-75

Kristensen, L., Can a cup anemometer 'underspeed'? A heretical question. Boundary-Layer Meteorol. (2002) **103** , 163-172

MacCready, P.B., 1966: Mean Wind Speed Measurements in Turbulence. J. Appl. Meteorol., **5**, 219-225.

Manier, G. and W. Benesch, 1977: Häufigkeitsverteilungen der Windgeschwindigkeit bis 250 m Höhe für die Bundesrepublik Deutschland. Meteorol. Rdsch., **30**, 144-152.

Panofsky H.A., H. Tennekes, D.H. Lenshow and J.C. Wyngaard (1977). The characteristics of turbulent components in the surface layer under convective situations. Boundary Layer Meteorol. 11, 355- 361,

Reitebuch, O., 1999: SODAR-Signalverarbeitung von Einzelpulsen zur Bestimmung hochaufgelöster Windprofile. Schriftenreihe des Institut für Atmos. Umweltforschung in Garmisch-Partenkirchen, Vol. **62**. 175 pp. (Available from: Shaker Verlag GmbH, Postfach 1290, D-52013 Aachen, ISBN: 3-8265-6208-9)

Reitebuch, O. and S. Vogt, 1998: Comparison of horizontal and vertical wind components measured by the METEK DSDR3x7 SODAR and tower instruments. In: Mursch-Radlgruber, E. and P. Seibert (Eds.): Proc. 9th ISARS, Vienna, Österr. Beitr. Meteorol. Geophys., **17**, 143-146.

Salomons, E. M. (2001). *Computational atmospheric acoustics.* Dordrecht, Kluwer Academic Publisher.

Simmons, W. R.; Wescott, J. W.; Hall, F. F., Jr., 1971: Acoustic echo sounding as related to air pollution in urban environments. NOAA TR ERL 216-WPL 17, Boulder, CO, 77 pp.

Stull, R.B., 1988: An Introduction to Boundary Layer Meteorology. Kluwer Acad. Publ. Dordrecht. 666 pp.

Traub, S. and B. Kruse, 1996: Winddaten für Windenergienutzer. Selbstverlag des Deutschen Wetterdienstes, Offenbach am Main. 455pp.

Westermann, D., 1996: Overspeeding - über das eigentümliche Tiefpaßverhalten von Schalensternanemometern. DEWI Magazin, Nr. 9, August 1996, 56-63.

Wieringa, J., 1989: Shapes of annual frequency distributions of wind speed observed on high meteorological masts. Bound.-Lay. Meteorol., **47**, 85-110.

Wippermann, F., 1973: Numerical Study on the Effects Controlling the Low-Level Jet. Beitr. Phys. Atmosph., **46**, 137-154.

Bibliographic Data Sheet **Risø-R-1410(EN)**

Title and authors

On the theory of SODAR measurement techniques

Ioannis Antoniou (ed.), Hans E. Jørgensen (ed.), Frank Ormel, Stuart Bradley, Sabine von Hünerbein, Stefan Emeis, Günter Warmbier,

ISBN	ISSN
87-550-3217-6 87-550-3218-4 (Internet)	0106-2840

Dept. or group	Date
TEM-VEA Wind Energy Department	Monday, 07 April 2003

Groups own reg. number(s)	Project/contract No.
1125117-01	NNE5-2001-297

Pages	Tables	Illustrations	References
59	2	45	31

Abstract

The need for alternative means to measure the wind speed for wind energy purposes has increased with the increase of the size of wind turbines. The cost and the technical difficulties for performing wind speed measurements has also increased with the size of the wind turbines, since it is demanded that the wind speed has to be measured at the rotor centre of the turbine and the size of both the rotor and the hub height have grown following the increase in the size of the wind turbines. The SODAR (SOund Detection And Ranging) is an alternative to the use of cup anemometers and offers the possibility of measuring both the wind speed distribution with height and the wind direction.

At the same time the SODAR presents a number of serious drawbacks such as the low number of measurements per time period, the dependence of the ability to measure on the atmospheric conditions and the difficulty of measuring at higher wind speeds due to either background noise or the neutral condition of the atmosphere.

Within the WISE project (EU project number NNE5-2001-297), a number of work packages have been defined in order to deal with the SODAR. The present report is the result of the work package 1. Within this package the objective has been to present and achieve the following:

- An accurate theoretic model that describes all the relevant aspects of the interaction of the sound beam with the atmosphere in the level of detail needed for wind energy applications.
- Understanding of dependence of SODAR performance on hard- and software configuration.
- Quantification of principal difference between SODAR wind measurement and wind speed measurements with cup anemometers with regard to power performance measurements.

Descriptors INIS/EDB

ACOUSTIC MEASUREMENTS; ANEMOMETERS; COMPARATIVE EVALUATIONS; PERFORMANCE; VELOCITY; WIND; WIND TURBINES